

The community-centered freshwater biogeochemistry model unified RIVE v1.0: a unified version for water column

Shuaitao Wang¹, Vincent Thieu¹, Gilles Billen¹, Josette Garnier¹, Marie Silvestre², Audrey Marescaux¹, Xingcheng Yan¹, and Nicolas Flipo³

¹Sorbonne Université, CNRS, EPHE, UMR Metis, 75005 Paris, France

²Sorbonne Université, CNRS, FR3020 FIRE, 75005 Paris, France

³Mines Paris, PSL University, Center for geosciences and geoen지니어ing, 77300 Fontainebleau, France

Correspondence: Shuaitao Wang (shuaitao.wang@sorbonne-universite.fr; shuaitaowang@outlook.com)

Abstract.

Research on mechanisms of organic matter degradation, bacterial activities, phytoplankton dynamics, and other processes has led to the development of numerous sophisticated water quality models. The earliest model, dating back to 1925, was based on first-order kinetics for organic matter degradation. The community-centered freshwater biogeochemistry model RIVE was initially developed in 1994 and has subsequently been integrated into several software programs such as Seneque-Riverstrahler, pyNuts-Riverstrahler, PROSE/PROSE-PA and Barman. After 30 years of research, the use of different programming languages including Qbasic, Visual Basic, Fortran, ANSIC and Python, as well as parallel evolution and the addition of new formalisms, raise questions about their comparability.

This paper presents a unified version of the RIVE model for the water column, including formalisms for bacterial communities (heterotrophic and nitrifying), primary producers, zooplankton, nutrients, inorganic carbon, and dissolved oxygen cycles. The unified RIVE model is open source and implemented in Python 3 to create pyRIVE 1.0, and in ANSIC to create C-RIVE 0.32. The organic matter degradation module is validated by simulating batch experiments. The comparability of the pyRIVE 1.0 and C-RIVE 0.32 softwares is verified by modeling a river stretch case study. The case study considers the full biogeochemical cycles (microorganisms, nutrients, carbon, and oxygen) in the water column, as well as the effects of light and water temperature. The results show that the simulated concentrations of all state variables, including microorganisms and chemical species, are very similar for pyRIVE 1.0 and C-RIVE 0.32. This open-source project highly encourages contributions from the freshwater biogeochemistry community to further advance the project and achieve common objectives.

1 Introduction

Modeling of the water quality of a freshwater system (river, lake or reservoir) is critical to understand and manage its functioning. The functioning of a freshwater system is the results of complex interrelated biogeochemical processes. The first water quality model developed by Streeter and Phelps (1925) describes the degradation of organic matter (OM) in river. The organic matter, measured globally by biochemical oxygen demand in 5 days (BOD₅), is considered to be degraded according to a first-order kinetics. Although dating back more than a century (the study was completed in 1915, but publication was delayed

to 1925 due to World War I (Hellweger, 2015)), this model is still widely used to represent the dynamics of organic matter in
25 water quality modeling. (Hellweger, 2015).

While the role of microorganisms in the degradation of organic matter has been acknowledged since the end of the 19th
century, there is an important limitation of this type of representation. The microbiological nature of the organic matter degra-
dation process and the bacterial population dynamics intrinsically involved are completely obscured. They are implicitly taken
into account only through a biodegradability constant of organic matter and its dependence on temperature. Microbial biogeo-
30 chemical work in the 1980s-1990s led to the elucidation of the detailed mechanisms of the organic matter degradation process
and the associated heterotrophic bacterial activities (Fuhrman and Azam, 1982; Azam et al., 1983; Somville and Billen, 1983;
Servais et al., 1985; Rego et al., 1985; Fontigny et al., 1987; Servais et al., 1987; Billen et al., 1988; Servais et al., 1989;
Billen et al., 1990; Garnier et al., 1992a, b). This new corpus of knowledge led to the development and the formulation of the
biogeochemical model RIVE (Billen et al., 1994; Garnier and Billen, 1994). It is capable of simulating the degradation of OM
35 in freshwater systems and the associated oxygen consumption by bacterial activities, which is more realistic than the model
of Streeter and Phelps (1925). In RIVE model, the **HSB** model (Billen and Servais, 1989; Billen, 1991) is used to represent
the degradation of organic matter and heterotrophic bacterial activities. This model simulates the exoenzymatic hydrolysis of
particulate and dissolved organic matter (split into biodegradable and refractory pools), including **H**igh weight polymers, into
small monomeric **S**ubstrates. These substrates are subsequently assimilated by **B**acteria for their growth and respiration.

40 Apart from the degradation of organic matter, the AQUAPHY model (Lancelot et al., 1991) is been used for simulating
the dynamics of phytoplankton in the RIVE model (Billen et al., 1994). The model simulates explicitly photosynthesis of
phytoplankton, growth, mortality and respiration processes. In addition to water temperature, the photosynthesis depends on
the light intensity while the growth is controlled by nutrients availability and small organic metabolites. The small organic
metabolites are formed either directly by photosynthesis or by catabolism of reserve products. This conceptualization allows
45 for a growth of phytoplankton during dark periods. In addition, the model also introduces a limiting factor of nutrients in the
growth of phytoplankton and considers the cycling of nutrients during the life cycle of phytoplankton.

Since its initial development by Billen et al. (1994), the RIVE model co-exists within several softwares (Tab. A1) developed
for different aquatic compartments and supported by the PIREN-Seine program (<https://www.piren-seine.fr/>). The RIVE model
was firstly applied in river systems using the Riverstrahler drainage network approach (Billen et al., 1994; Garnier et al.,
50 1995). It was initially coded in Qbasic, and later on piloted by a GIS graphical interface Seneque-Riverstrahler (Visual Basic,
(Ruelland et al., 2007)). And it is now fully integrated within the pyNuts-Riverstrahler (<https://gitlab.in2p3.fr/rive/pynuts/>,
Python framework (Thieu et al., 2017)). It can model the biogeochemical functioning of hydrographic networks at scales
ranging from local to continental. RIVE model was also applied to lentic freshwater systems like regulated reservoirs (BarMan
software (Garnier et al., 2000; Thieu et al., 2006; Yan et al., 2022a), Tab. A1.) or simulating hydro-biodynamic functioning
55 of highly human impacted river system (PROSE software – Even et al. (1998, 2004, 2007); Flipo et al. (2004); Vilmin et al.
(2015b), and PROSE-PA software – Wang et al. (2019, 2023a), <https://gitlab.com/prose-pa/prose-pa>, developed in ANSI C
coupled with a self developed lex and yacc parser, Tab. A1.). The RIVE model is also coupled with the Soil & Water Assessment
Tool (SWAT) to simulate the water quality of the Vienne basin, France (Manteaux et al., 2023, submitted) and incorporated

into the QUAL-NET model (Minaudo et al., 2018) to simulate river eutrophication in the drainage network of the Middle Loire River Corridor, France. Moreover, the RIVE model is implemented into the VEMALA V3 model for simulating phosphorus and nitrogen loading in the Finnish watersheds (Korppoo et al., 2017).

Based on above implementations, different versions of the RIVE model code have simulated successfully a large variety of freshwater systems (lake or reservoirs, river systems) across the world. The parameter values were determined through laboratory experiments or calibrated with observation data (Garnier et al., 1992a; Servais and Garnier, 1993; Garnier and Billen, 1994; Billen et al., 1994; Garnier et al., 1995). These applications (Tab. A1) were carried out for different networks and scales as well as various degrees of anthropogenic impacts in a wide climatic gradient using either Riverstrahler (possibly with its Seneque or pyNuts environments) or PROSE/PROSE-PA, such as the Seine River (France) (Billen et al., 1994; Garnier et al., 1995; Even et al., 1998, 2004, 2007; Billen et al., 2007; Servais et al., 2007; Thieu et al., 2009, 2010; Vilmin et al., 2015b, a; Aissa-Grouz et al., 2016; Vilmin et al., 2016; Desmit et al., 2018; Vilmin et al., 2018; Romero et al., 2019; Marescaux et al., 2020; Wang et al., 2022), the Danube river (Romania and Bulgaria) (Garnier et al., 2002), the Red River (China and Vietnam) (Le et al., 2010; Phuong Quynh et al., 2014; Le et al., 2015; Nguyen et al., 2016) and its tributary Day-Nhue River (Luu et al., 2021), the Lule and Kalix rivers (Sweden) (Sferratore et al., 2008), the Scheldt river (Belgium and Netherlands) (Billen et al., 2005; Thieu et al., 2009), the Zenne River (Belgium) (Garnier et al., 2013), the Mosel River (Germany) (Garnier et al., 1999a), the Somme River (France) (Thieu et al., 2009, 2010), the Loire River (France) (Garnier et al., 2018a), the Lot River (France) (Garnier et al., 2018b) and the Orgeval watershed (France) (Flipo et al., 2004, 2007; Garnier et al., 2014). Moreover, the RIVE model has been applied to the stagnant systems also (e.g. sand-pit lake (Lake Crétail - France, (Garnier and Billen, 1994)), reservoirs (Marne, Aube, Seine - France, (Garnier et al., 2000; Yan et al., 2022a))).

After 30 years of research, the parallel evolutions of these codes, the numerical adaptations inherent in programming languages (Qbasic, Visual Basic, Fortran, Python and ANSI C) and the addition of new formalisms, raise the question of their comparability. The identification of a unified version of RIVE model is then necessary. A project aiming at unifying these RIVE implementations was undertaken. The unified version brings together all recent developments, especially the ones achieved with Python and ANSI C programming languages. This action will strengthen the collaboration of the research teams involved in the development of the model. This paper presents then a unified version of RIVE for water column (called unified RIVE v1.0) with a presentation of the formalisms for the biogeochemical cycles. That integrates the bacterial communities (heterotrophic and nitrifying), primary producers, zooplankton and fate of detritic organic matter either particulate or dissolved as well as biodegradable and refractory, and the associated nutrients and dissolved oxygen cycles. The most recent developments on the modeling of inorganic forms of carbon are also presented. The unified RIVE v1.0 included in pyRIVE 1.0 (tested with Python 3 versions up to 3.10 release) and C-RIVE 0.32 is open source and therefore available to the scientific community. A numerical experiment is then introduced to evaluate the comparability of the pyRIVE 1.0 and C-RIVE 0.32 through a systematic comparison of simulations produced under controlled conditions. We thus establish a reference framework to evaluate different implementations (programming languages, performance - comparability) of the unified RIVE v1.0 formulation, that continues to evolve in several water quality models.

2 Model description

The unified RIVE v1.0 model simulates the cycling of carbon, nutrients and oxygen within an freshwater system (river, lake, reservoir). Biogeochemical cycles are simulated with a community-centered or agent-based model. That means that the freshwater system functioning is explicitly modeled, taking into consideration the activities of microorganisms such as phytoplankton, zooplankton, heterotrophic bacteria, and nitrifying bacteria. Additionally, it accounts for physical processes like oxygen reaeration and dilution. This modeling approach is developed in relation to water temperature, macronutrients and organic matter, (particulate, dissolved, and biodegradable fractions). The organic matter degradation, nitrifying bacteria dynamics, primary producer dynamics, zooplankton dynamics, nutrients and inorganic carbon cycling are described subsequently. A high number of model parameters are used to characterize the microorganisms' properties and most of them have been determined through field or laboratory experiments under controlled conditions. This paper presents a focus on the conceptualization of the unified RIVE v1.0 model in water column exclusively. While RIVE model does have applications for sediment dynamics and its interaction with the water column (Even et al., 2004; Thouvenot et al., 2007; Billen et al., 2015; Vilmin et al., 2015a, 2016; Yan et al., 2022b), relevant community-centred efforts need to be made in future work, which is not the focus of this study.

2.1 Organic matter degradation

The mechanisms of organic matter degradation by the activity of heterotrophic bacteria are represented using **HSB** model (Billen and Servais, 1989; Billen, 1991). It contains three variables: **H**, High weight polymers (large molecules) which form the majority of dissolved and particulate organic matter, but must be exoenzymatically hydrolyzed to be accessible to heterotrophic bacteria; **S**, small monomeric Substrates (SMS), directly accessible to microbial uptake; **B**, heterotrophic Bacteria that absorbs the substrates for their growth and respiration (Fig. 1). In diagrams of this paper (for instance HSB model, Fig. 1), the state variables are represented by circles and represent either concentrations or stocks entering and leaving the (biogeochemical) processes. The biogeochemical processes are represented by squares.

The high weight polymer (total organic carbon) is conceptually divided for each phase (Dissolved (HD) and Particulate (HP)), into three pools. Each pool is characterized by a specific biodegradability: (1) rapidly biodegradable in 5 days (HD₁ and HP₁); (2) slowly biodegradable in 45 days (HD₂ and HP₂); (3) refractory (HD₃ and HP₃).

2.1.1 Heterotrophic bacteria dynamics

The dynamic of heterotrophic bacteria is explicitly simulated: growth, mortality, respiration etc. The growth of heterotrophic bacteria depends on water temperature and the availability of small monomeric substrate (SMS). The dependence is represented by Monod equation (Monod, 1949). A maximal substrate uptake rate at 20 °C ($b_{max20,hb}$) and a bacterial growth yield (Y_{hb}) are used to calculate the growth rate of heterotrophic bacteria (μ_{hb_i}) (Eq. (3)). The fraction of uptake not used for growth

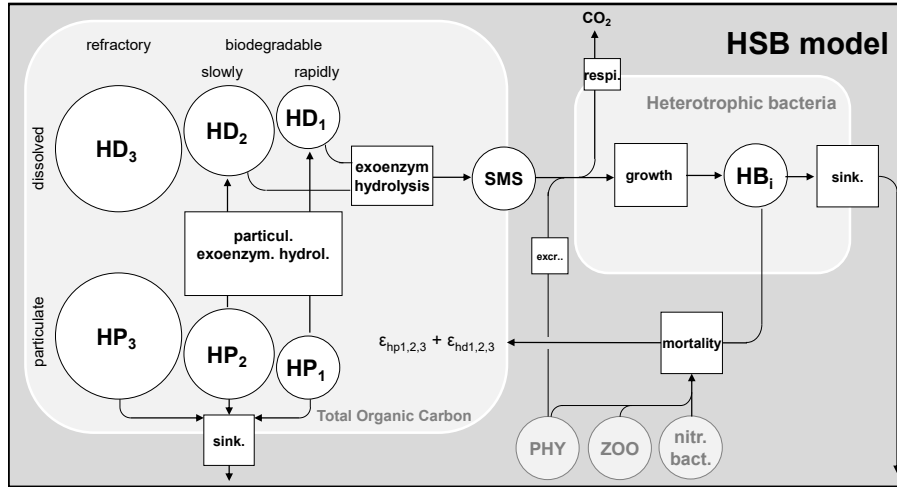


Figure 1. Flowchart of HSB model. HD: dissolved high weight polymer; HP: particulate high weight polymer; SMS: small monomeric substrate; HB: heterotrophic bacteria; PHY: phytoplankton; ZOO: zooplankton; nitr. bact.: Nitrifying bacteria; extr.: excretion of phytoplankton; sink.: sinking. respi.: respiration; $\epsilon_{hp1,2,3}$ and $\epsilon_{hd1,2,3}$: Proportion to convert dead biomass to HP and HD

$(1 - Y_{hb})$ is respired.

$$b_{hb_i} = b_{max20,hb_i} f(T)_{hb_i} \frac{[SMS]}{[SMS] + K_{sms,hb_i}} \quad (1)$$

$$f(T)_{hb_i} = \frac{e^{-\frac{(T-T_{opt,hb_i})^2}{\sigma_{hb_i}^2}}}{e^{-\frac{(20-T_{opt,hb_i})^2}{\sigma_{hb_i}^2}}} \quad (2)$$

$$125 \quad \mu_{hb_i} = Y_{hb_i} b_{hb_i} \quad (3)$$

With b_{hb_i} : Effective substrate uptake rate of the i^{th} species of heterotrophic bacteria, [h^{-1}]

b_{max20,hb_i} : Maximal substrate uptake rate of the i^{th} species of heterotrophic bacteria at 20 °C, [h^{-1}]

$[SMS]$: Small monomeric substrate concentration, [$mgC L^{-1}$]

K_{sms,hb_i} : Half-saturation constant for small monomeric substrate of the i^{th} species of heterotrophic bacteria, [$mgC L^{-1}$]

130 $f(T)_{hb_i}$: Water temperature weight of the i^{th} species of heterotrophic bacteria at T °C, [-]

T_{opt,hb_i} : Optimal temperature of the i^{th} species of heterotrophic bacteria for its growth, [°C]

σ_{hb_i} : Range of temperature for the i^{th} species of heterotrophic bacteria, [°C]

Y_{hb_i} : Bacterial growth yield of the i^{th} species of heterotrophic bacteria, [-]

μ_{hb_i} : Effective growth rate of the i^{th} species of heterotrophic bacteria, [h^{-1}]

135 A sinking velocity (vs_{hb}) is associated to each particulate species to represent particulate sinking by gravity. The mortality of heterotrophic bacteria is simulated by a first order kinetics (Eq. (4)). The dead biomass of living species is converted into

varying types of organic matter content, including both dissolved and particulate forms, based on specified proportions (ϵ_{hd} and ϵ_{hp} , Fig. 1).

$$\frac{d[HB_i]}{dt} = (\mu_{hb_i} - k_{d20,hb_i} f(T)_{hb_i} - k_{sink,hb_i}) [HB_i] \quad (4)$$

$$140 \quad k_{sink,hb_i} = \frac{vs_{hb_i}}{depth}$$

With μ_{hb_i} : Effective growth rate of the i^{th} species of heterotrophic bacteria, [h^{-1}]

k_{d20,hb_i} : Mortality rate of the i^{th} species of heterotrophic bacteria at 20 °C, [h^{-1}]

k_{sink,hb_i} : Sinking rate of the i^{th} species of heterotrophic bacteria, [h^{-1}]

$[HB_i]$: Biomass concentration of the i^{th} species of heterotrophic bacteria, [$mgC L^{-1}$]

145 $f(T)_{hb_i}$: Water temperature weight at T °C defined by equation (2), [-]

vs_{hb_i} : Sinking velocity of the i^{th} species of heterotrophic bacteria, [$m h^{-1}$]

$depth$: Water depth, [m]

2.1.2 Hydrolysis of high weight polymer

150 The particulate biodegradable high weight polymer (HP_1 and HP_2) is firstly hydrolyzed to the dissolved biodegradable high weight polymer (HD_1 and HD_2). The dissolved biodegradable high weight polymer is then hydrolyzed exoenzymatically to small monomeric substrate (Fig. 1). The hydrolysis of HP is represented by a first order kinetics (Eq. (5)) while a Michaelis-Menten function (Michaelis and Menten, 1913) is used to express the exoenzymatic hydrolysis of HD (Eq. (6)).

$$\frac{d[HP_i]}{dt} = -k_{hp_i} * [HP_i] + \left(\sum_j k_{d20,j} f(T)_j [LS]_j \right) \epsilon_{hp_i} - k_{sink,hp_i} [HP_i] \quad (5)$$

155 With $[HP_i]$: Concentration of particulate high weight polymer, $i \in \{1, 2\}$, [$mgC L^{-1}$]

k_{hp_i} : Hydrolysis rate of HP_i , $i \in \{1, 2\}$, [h^{-1}]

$f(T)_j$: Water temperature weight of the j^{th} living species at T °C defined like the equation (2), [-]

$k_{d20,j}$: Mortality rate of the j^{th} living species (such as phytoplankton, zooplankton, bacteria etc.) at 20 °C, [h^{-1}]

$[LS]_j$: Concentration of the j^{th} living species, [$mgC L^{-1}$]

160 ϵ_{hp_i} : Proportion to convert the dead biomass to HP_i , $i \in \{1, 2\}$, [-]

k_{sink,hp_i} : Sinking rate for HP_i , $i \in \{1, 2\}$, [h^{-1}]

$$\frac{d[HD_i]}{dt} = - \sum_k (e_{max20,hd_i,hb_k} f(T)_k \frac{[HD_i]}{[HD_i] + K_{hd_i,hb_k}} [HB_k]) + k_{hp_i} * [HP_i] + \left(\sum_j k_{d20,j} f(T)_j [LS]_j \right) \epsilon_{hd_i} \quad (6)$$

With $[HD_i]$: concentration of dissolved high weight polymer, $i \in \{1, 2\}$, [$mgC L^{-1}$]

e_{max20,hd_i,hb_k} : Maximum hydrolysis rate of HD_i at 20 °C related to HB_k , $i \in \{1, 2\}$, [h^{-1}]

- 165 $f(T)_k$: Water temperature weight of the k^{th} species of heterotrophic bacteria at T °C (Eq. (2)), [-]
 K_{hd_i, hb_k} : Half-saturation constant for HD_i related to HB_k , $i \in \{1, 2\}$, [mgC L^{-1}]
 $[HB_k]$: Concentration of the k^{th} species of heterotrophic bacteria, [mgC L^{-1}]
 $k_{d20,j}$: Mortality rate of the j^{th} living species (such as phytoplankton, zooplankton, bacteria etc.) at 20 °C, [h^{-1}]
 $f(T)_j$: Water temperature weight of the j^{th} living species at T °C defined like the equation (2), [-]
- 170 $[LS]_j$: Concentration of the j^{th} living species, [mgC L^{-1}]
 ϵ_{hd_i} : Proportion to convert the dead biomass to HD_i , $i \in \{1, 2\}$, [-]

2.2 Nitrifying bacteria dynamics

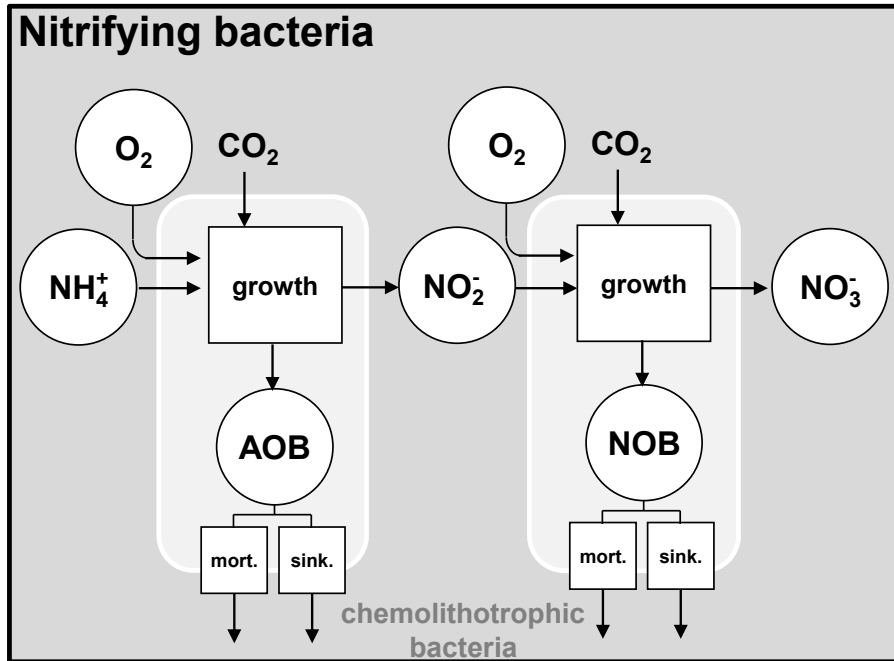


Figure 2. Nitrifying bacteria dynamics. AOB: ammonia-oxidizing bacteria; NOB: nitrite-oxidizing bacteria; mort.: mortality; sink.: sinking

The unified RIVE v1.0 model includes the description of the nitrification microbial process, mediated by two types of nitrifying bacteria. They are respectively responsible for the production of nitrite ($\text{NH}_4^+ + \frac{3}{2}\text{O}_2 \longrightarrow \text{NO}_2^- + 2\text{H}^+ + \text{H}_2\text{O}$) and nitrate ($\text{NO}_2^- + \frac{1}{2}\text{O}_2 \longrightarrow \text{NO}_3^-$). The nitrifying bacteria get energy by oxidizing NH_4^+ (ammonium) and NO_2^- (nitrite) for their growth. These two bacteria are named AOB (ammonia-oxidizing bacteria) and NOB (nitrite-oxidizing bacteria) respectively (Brion and Billen, 1998). The growth of nitrifying bacteria is limited by the availability of ammonium, nitrite and oxygen,

which is represented with Monod functions (Eq. (7)). The effect of water temperature is taken into account also.

$$\mu_{aob} = \mu_{max20,aob} f(T)_{aob} \left(\frac{[NH_4^+]}{[NH_4^+] + K_{nh_4,aob}} \right) \left(\frac{[O_2]}{[O_2] + K_{o_2,aob}} \right) \quad (7)$$

$$180 \quad \mu_{nob} = \mu_{max20,nob} f(T)_{nob} \left(\frac{[NO_2^-]}{[NO_2^-] + K_{no_2,nob}} \right) \left(\frac{[O_2]}{[O_2] + K_{o_2,nob}} \right) \quad (8)$$

With μ_{aob} and μ_{nob} : Effective growth rate of AOB and NOB, [h^{-1}]

$\mu_{max20,aob}$ and $\mu_{max20,nob}$: Maximal growth rates of AOB and NOB at 20 °C, respectively, [h^{-1}]

$f(T)_{aob}$ and $f(T)_{nob}$: Water temperature weight at T °C defined like the equation (2), [-]

$K_{nh_4,aob}$ and $K_{no_2,nob}$: Half-saturation constants for NH_4^+ (AOB) and for NO_2^- (NOB), [$mgN L^{-1}$]

185 $K_{o_2,aob}$ and $K_{o_2,nob}$: Half-saturation constants for oxygen (AOB and NOB), [$mgO_2 L^{-1}$]

The mortality and sinking of nitrifying bacteria are simulated the same way than for other living species.

$$\frac{d[AOB]}{dt} = (\mu_{aob} - k_{d20,aob} f(T)_{aob} - k_{sink,aob}) [AOB] \quad (9)$$

$$\frac{d[NOB]}{dt} = (\mu_{nob} - k_{d20,nob} f(T)_{nob} - k_{sink,nob}) [NOB] \quad (10)$$

With μ_{aob} and μ_{nob} : Effective growth rate of AOB and NOB defined by (7) and (8), [h^{-1}]

190 $k_{d20,aob}$ and $k_{d20,nob}$: Mortality rate of AOB and NOB at 20 °C, [h^{-1}]

$k_{sink,aob}$ and $k_{sink,nob}$: Sinking rate of AOB and NOB, [h^{-1}]

$f(T)_{aob}$ and $f(T)_{nob}$: Water temperature weight at T °C defined like the equation (2), [-]

$[AOB]$ and $[NOB]$: Concentrations of AOB and NOB, [$mgC L^{-1}$]

2.3 Primary producer dynamics

195 The behavior of primary producers is represented using the AQUAPHY model (Lancelot et al., 1991). Biomass of a phytoplankton species is composed of three different cellular constituents (Fig. 3):

(a) The structural and functional macromolecules of the cell, **F**; mainly proteins, chlorophyll and structural lipids (such as membranes)

(b) Polysaccharides playing the role of reserve products, **R**;

200 (c) Monomeric (amino acids) and oligomeric precursors for macromolecular synthesis, **S**

At any time, the biomass of the j^{th} phytoplankton species ($mgC L^{-1}$), $[PHY]_j$, is equal to the sum of the three internal constituents (Eq. (11)), $[F]_j$, $[R]_j$, $[S]_j$:

$$[PHY]_j = [F]_j + [R]_j + [S]_j \quad (11)$$

The most common way of measuring phytoplankton biomass is using the chlorophyll *a* concentration ($\mu gchl a L^{-1}$). A
205 carbon/chlorophyll *a* ratio of 35 $mgC/\mu gchl a$ is therefore considered to convert experimental data into phytoplankton biomass.

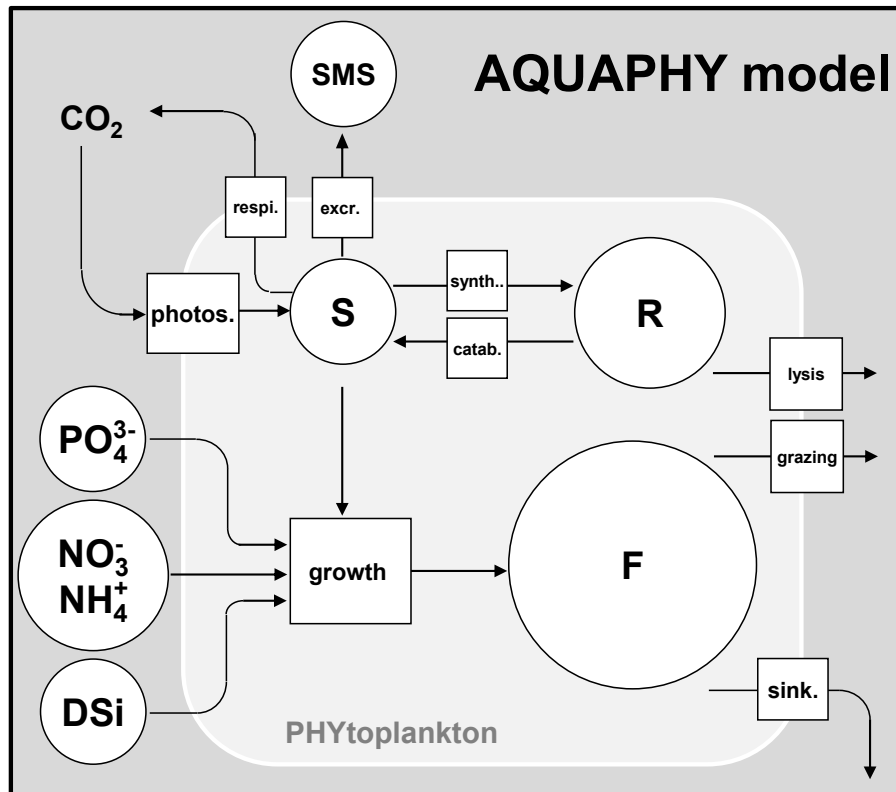


Figure 3. Description of AQUAPHY model. F: functional macromolecules of the cell; R: reserve products; S: Monomeric (amino acids) and oligomeric precursors for macromolecular synthesis. Phytoplankton biomass equals to the sum of the three cellular constituents (F, R, S). SMS: small monomeric substrate. photos.: photosynthesis; respi.: respiration; excr.: excretion; synth.: synthesis; catab.: catabolysis; sink.: sinking

The initial proportions of different constituents (F, R, S) are fixed (Lancelot et al., 1991). They are only used to determine the initial concentrations of the three cellular constituents and their concentrations in incoming water fluxes for each phytoplankton species. According to Lancelot et al. (1991), the structural and functional macromolecules of the cell ($[F]_j$) account for about 85% of the phytoplankton biomass ($[PHY]_j$), while the reserve products ($[R]_j$) account for about 10% of the biomass. The remainder (5%) of the biomass constitutes the small precursors for macromolecules synthesis ($[S]_j$). These proportions of F, S, R are updated at each time step for each phytoplankton species.

2.3.1 Photosynthesis

The photosynthesis process forms small precursors (**S**) by fixing carbon dioxide. Its rate is determined by the photosynthesis-irradiance relationship (Platt et al., 1980) including three parameters (Eq. (12)) and the active irradiance ($I(z)$, $\mu\text{E m}^{-2} \text{s}^{-1}$).

$$215 \quad P(z)_{phy_j} = P_{max20,phy_j} f(T)_{phy_j} \left(1 - e^{-\frac{\alpha_{phy_j} I(z)}{P_{max20,phy_j} f(T)}}\right) e^{-\frac{\beta_{phy_j} I(z)}{P_{max20,phy_j} f(T)}} \quad (12)$$

$$(13)$$

with $P(z)_{phy_j}$: Photosynthesis rate of the j^{th} phytoplankton species at water depth z m, [h^{-1}]

P_{max20,phy_j} : Maximal photosynthesis rate of the j^{th} phytoplankton species at 20 °C, [h^{-1}]

$f(T)_{phy_j}$: Water temperature weight of the j^{th} phytoplankton species at T °C defined like the equation (2), [-]

$$220 \quad \alpha_{phy_j}: \text{Photosynthetic efficiency of the } j^{th} \text{ phytoplankton species, } [\text{h}^{-1} (\mu\text{E m}^{-2} \text{s}^{-1})^{-1}]$$

β_{phy_j} : Photoinhibition capacity of the j^{th} phytoplankton species, [$\text{h}^{-1} (\mu\text{E m}^{-2} \text{s}^{-1})^{-1}$]

$I(z)$: Photosynthetically Active Radiation (PAR) or active irradiance in water column at depth z m, [$\mu\text{E m}^{-2} \text{s}^{-1}$] or [W m^{-2}]

The averaged photosynthesis rate of the j^{th} phytoplankton species over water column is obtained by integrating $P(z)$.

$$p_{phy_j} = \frac{\int_0^{depth} P(z)_{phy_j} dz}{depth} \quad (14)$$

$$225 \quad \text{where } depth \text{ is the water height (m) and } p_{phy_j} \text{ is the averaged photosynthesis rate over water column (h}^{-1}\text{).}$$

The active irradiance at water depth z m ($I(z)$) follows the Beer–Lambert law (Eq. (15)). The decrease of active irradiance from water surface to water bottom is represented by light extinction coefficient (η). The extinction coefficient is composed of three parts: pure water (η_{base}), suspended solid (η_{ss}) and algal self-shading (η_{chla}).

$$I(z) = I_0 e^{-\eta z} \quad (15)$$

$$230 \quad \eta = \eta_{base} + \eta_{chla}[chla] + \eta_{ss}[SS]$$

with $I(z)$: Active irradiance at water depth z m, [$\mu\text{E m}^{-2} \text{s}^{-1}$] or [W m^{-2}]

I_0 : Photosynthetically Active Radiation (PAR), or active irradiance at water surface, measured by the Photosynthetic Photon¹ Flux Density (PPFD) [$\mu\text{E m}^{-2} \text{s}^{-1}$] or [W m^{-2}]

η : Light extinction coefficient, [m^{-1}]

$$235 \quad \eta_{base}: \text{Light extinction coefficient related to pure water, } [\text{m}^{-1}]$$

η_{chla} : Linear algal self-shading light extinction coefficient, [$\text{m}^{-1} (\mu\text{gchla L}^{-1})^{-1}$]

η_{ss} : Light extinction coefficient related to suspended solid, [$\text{m}^{-1} (\text{mg L}^{-1})^{-1}$]

[$chla$]: Total chlorophyll a concentration, [$\mu\text{gchla L}^{-1}$]

[SS]: Suspended solid concentration, [mg L^{-1}]

¹Photons within the range of visible light between 400 and 700 nm

240 2.3.2 Growth

The growth of phytoplankton involves the transformation of small precursors (**S**) into structural and functional macromolecules (**F**), which also requires the uptake of dissolved inorganic nutrients (nitrogen - N, phosphorus - P, silicon - Si) from the environment (Fig. 3). The nutrients can potentially limit phytoplankton growth if their quantities are insufficient. The limitation of nutrients is represented using multiple Monod functions (Eq. (16)). The maximum growth rate (μ_{max,F_j}) is itself weighted
 245 by a limitation based on the availability of small precursors (**S**). The limitation by dissolved silica (DSi) is applied only for diatoms (DIA).

$$\mu_{F_j} = \mu_{max20,F_j} f(T)_{phy_j} \left(\frac{\frac{[S_j]}{[F_j]}}{\frac{[S_j]}{[F_j]} + K_{S,phy_j}} \right) Nut_lim \quad (16)$$

$$Nut_lim = \min\left(\frac{[DIN]}{[DIN] + K_{N,phy_j}}, \frac{[DIP]}{[DIP] + K_{P,phy_j}}, \frac{[DSi]}{[DSi] + K_{Si,phy_j}}\right) \quad (17)$$

$$\text{or } Nut_lim = \min\left(\frac{[DIN]}{[DIN] + K_{N,phy_j}}, \frac{[DIP]}{[DIP] + K_{P,phy_j}}\right)$$

250 With μ_{F_j} : Effective growth rate of functional macromolecules for the j^{th} phytoplankton species, [h^{-1}]

μ_{max20,F_j} : Maximal growth rate of functional macromolecules for the j^{th} phytoplankton species at 20 °C, [h^{-1}]

$f(T)_{phy_j}$: Water temperature weight of the j^{th} phytoplankton species at T °C defined like the equation (2), [-]

$[S_j]$ and $[F_j]$: Concentrations of small precursors and functional macromolecules for the j^{th} phytoplankton species, [$mgC L^{-1}$]

K_{S,phy_j} : Half-saturation constant for small precursors of the j^{th} phytoplankton species, [-]

255 Nut_lim : Nutrients limiting factor, [-]

$[DIN]$, $[DIP]$ and $[DSi]$: Concentrations of dissolved inorganic nitrogen ($[DIN] = [NO_3^-] + [NH_4^+]$, $mgN L^{-1}$), dissolved inorganic phosphorus ($[DIP] = [PO_4^{3-}]$, $mgP L^{-1}$) and dissolved silica (DSi, $mgSi L^{-1}$)

K_{N,phy_j} and K_{P,phy_j} : Half-saturation constant for dissolved inorganic nitrogen and phosphorus of the j^{th} phytoplankton species, [$mgN L^{-1}$] and [$mgP L^{-1}$]

260 K_{Si,phy_j} : Half-saturation constant for dissolved silica in case of diatoms, [$mgSi L^{-1}$]

2.3.3 Respiration

The respiration rate of phytoplankton (r_{phy}) is divided into two components (Eq. (18)): one ($R_{m,phy}$) ensuring the survival of the cell (maintenance process), the other ($R_{\mu,phy}$) corresponding to energetic cost of growth.

$$r_{phy_j} = R_{m20,phy_j} f(T)_{phy_j} + \mu_{F_j} R_{\mu,phy_j} \quad (18)$$

265 with r_{phy_j} : Respiration rate of the j^{th} phytoplankton species, [h^{-1}]

R_{m20,phy_j} : Maintenance respiration rate of the j^{th} phytoplankton species at 20 °C, [h^{-1}]

$f(T)_{phy_j}$: Water temperature weight of the j^{th} phytoplankton species at T °C defined like the equation (2), [-]

R_{μ,phy_j} : Respiration for energetic cost of the j^{th} phytoplankton species, [-]

μ_{F_j} : Effective growth rate of the j^{th} phytoplankton species (Eq. (16)), [h^{-1}]

270 2.3.4 Excretion

Included later by Garnier et al. (1998), the phytoplankton excretion (e_{phy}) includes two terms: a constant excretion rate ($E_{cst,phy}$) and another that depends on the photosynthesis rate ($E_{phot,phy}$). The product of excretion is the small monomeric substrate (SMS), assimilated directly by heterotrophic bacteria for their growth and respiration (Fig. 1).

$$e_{phy_j} = E_{cst,phy_j} + p_{phy_j} E_{phot,phy_j} \quad (19)$$

275 With e_{phy_j} : Excretion rate of the j^{th} phytoplankton species, [h^{-1}]

E_{cst,phy_j} : Basic excretion rate of the j^{th} phytoplankton species, [h^{-1}]

E_{phot,phy_j} : Excretion of the j^{th} phytoplankton species related to photosynthesis, [-]

p_{phy_j} : Photosynthesis rate of the j^{th} phytoplankton species (Eq. (14)), [h^{-1}]

The variation of small monomeric substrate (SMS) can then be established (Eq. (20)).

$$280 \frac{d[SMS]}{dt} = hydr - \sum_i b_{hb_i} [HB_i] + \sum_j e_{phy_j} [F_j] \quad (20)$$

With $hydr$: Hydrolysis of the dissolved high weight polymer HD_1 and HD_2 (Eq. (6)), [$mgC L^{-1} h^{-1}$]

b_{hb_i} : Effective rate of substrate uptake by the i^{th} heterotrophic bacteria species (Eq. (3)), [h^{-1}]

$[HB_i]$: Biomass concentration of the i^{th} species of heterotrophic bacteria, [$mgC L^{-1}$]

e_{phy_j} : Effective excretion rate of the j^{th} phytoplankton species (Eq. (19)), [h^{-1}]

285 $[F_j]$: Concentration of functional macromolecules for the j^{th} phytoplankton species, [$mgC L^{-1}$]

2.3.5 Synthesis and catabolism of reserve products

The carbon fixed in the cell by photosynthesis forms small precursors (**S**) that can be transformed, either into functional macromolecules (**F**), or into reserve products (**R**). The synthesis of reserve products is limited by the $\frac{[S]}{[F]}$ ratio based on a

290 Michaelis-Menten like function (Eq. (21)).

$$s_{R,phy_j} = s_{R,max20,phy_j} f(T)_{phy_j} \frac{\frac{[S_j]}{[F_j]}}{\frac{[S_j]}{[F_j]} + K_{S,phy_j}} \quad (21)$$

With s_{R,phy_j} : Synthesis rate of reserve products of j^{th} phytoplankton species, [h^{-1}]

$s_{R,max20,phy_j}$: Maximal synthesis rate of reserve products of j^{th} phytoplankton species at 20 °C, [h^{-1}]

$f(T)_{phy_j}$: Water temperature weight of j^{th} phytoplankton species at T °C defined like the equation (2), [-]

295 $[S_j]$ and $[F_j]$: Concentrations of small precursors and functional macromolecules for the j^{th} phytoplankton species, [$mgC L^{-1}$]

K_{S,phy_j} : Half-saturation constant for small precursors of the j^{th} phytoplankton species, [-]

Reserve products (**R**) are likely to be catabolized to produce small precursors (**S**). A first order kinetic ($c_{R,phy}$, h^{-1}) is used to represent catabolism of reserve product.

2.3.6 Extinction of phytoplankton

300 Three ways of phytoplankton extinction are implemented in the unified RIVE v1.0: lysis, sinking and grazing by zooplankton (Sct. 2.4.1). The phytoplankton lysis is represented by a first order kinetics using a mortality rate ($k_{d20,phy}$, h^{-1}). For ease of presentation, all three processes are assumed in an overall extinction rate d_{phy} (h^{-1}).

$$d_{phy_j} = k_{d20,phy_j} f(T)_{phy_j} + k_{sink,phy_j} + \sum_i \frac{b_{zoo_i} [ZOO_i]}{\sum_{k=1}^{NS} [PHY_k]} \quad (22)$$

With d_{phy_j} : Extinction rate of the j^{th} phytoplankton species, [h^{-1}]

305 k_{d20,phy_j} : Mortality rate of the j^{th} phytoplankton species at 20 °C, [h^{-1}]

$f(T)_{phy_j}$: Water temperature weight of j^{th} phytoplankton species at T °C defined like the equation (2), [-]

k_{sink,phy_j} : Sinking rate of the j^{th} phytoplankton species, [h^{-1}]

b_{zoo_i} : Grazing rate of the i^{th} zooplankton species (Eq. (27), section 2.4.1), [h^{-1}]

$[ZOO_i]$: Zooplankton concentration of the i^{th} zooplankton species, [$mgC L^{-1}$]

310 $\sum_{k=1}^{NS} [PHY_k]$: Total phytoplankton concentration (with NS the Number of phytoplankton species grazed by zooplankton), [$mgC L^{-1}$]

2.3.7 Phytoplankton budgets

According to the processes related to phytoplankton (photosynthesis, growth, mortality etc.), the different budgets can be established for the j^{th} phytoplankton species as follows.

$$315 \quad \frac{d[S_j]}{dt} = (p_{phy_j} - r_{phy_j} - \mu_{F_j} - s_{R,phy_j})[F_j] + c_{R,phy_j}[R_j] - e_{phy_j}[F_j] - d_{phy_j}[S_j] \quad (23)$$

$$\frac{d[R_j]}{dt} = s_{R,phy_j}[F_j] - c_{R,phy_j}[R_j] - d_{phy_j}[R_j] \quad (24)$$

$$\frac{d[F_j]}{dt} = (\mu_{F_j} - d_{phy_j})[F_j] \quad (25)$$

$$\frac{d[PHY_j]}{dt} = (p_{phy_j} - r_{phy_j} - e_{phy_j})[F_j] - d_{phy_j}[PHY_j] \quad (26)$$

With: p_{phy_j} : Photosynthesis rate of the j^{th} phytoplankton species (Eq. (14)), [h^{-1}]

320 r_{phy_j} : Respiration rate of the j^{th} phytoplankton species (Eq. (18)), [h^{-1}]

μ_{F_j} : Growth rate of the j^{th} phytoplankton species (Eq. (16)), [h^{-1}]

s_{R,phy_j} : Synthesis rate of reserve products of the j^{th} phytoplankton species (Eq. (21)), [h^{-1}]

c_{R,phy_j} : Catabolysis rate of reserve products of the j^{th} phytoplankton species, [h^{-1}]

e_{phy_j} : Excretion rate of the j^{th} phytoplankton species (Eq. (19)), [h^{-1}]

325 d_{phy_j} : Extinction rate of the j^{th} phytoplankton species (Eq. (22)), [h^{-1}]

$[S_j]$, $[F_j]$ and $[R_j]$: Concentrations of $[S_j]$, $[F_j]$ and $[R_j]$ for the j^{th} phytoplankton species, [$mgC L^{-1}$]

$[PHY_j]$: Biomass concentration of the j^{th} phytoplankton species, [$mgC L^{-1}$]

2.4 Zooplankton dynamics

The zooplankton dynamics include the grazing on phytoplankton, the growth, the respiration, the mortality and the sinking (Fig. 4).

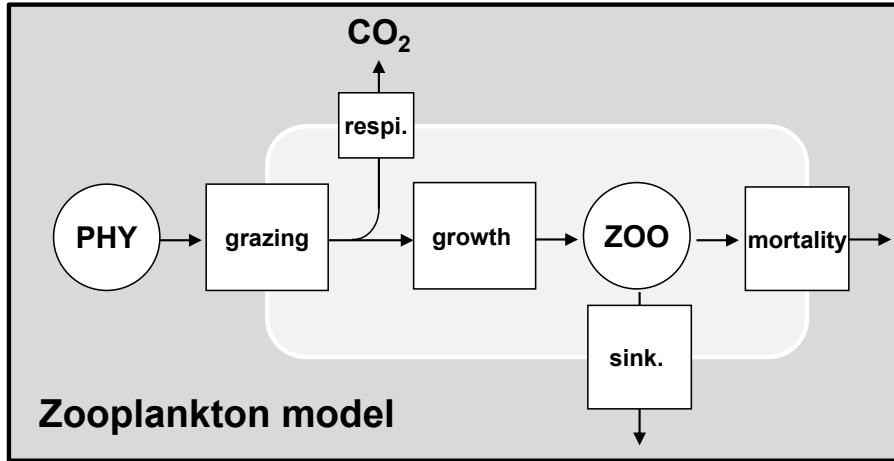


Figure 4. Dynamics of zooplankton. PHY: phytoplankton species; ZOO: zooplankton species; respi.: respiration; sink.: sinking

2.4.1 Grazing and Growth

The grazing on phytoplankton by zooplankton and the growth of zooplankton are expressed based on a maximal grazing rate at 20 °C ($b_{max20,zoo}$) limited by the phytoplankton biomass based on a Monod function (Eq. (27)). The grazing of zooplankton takes place only when the total phytoplankton biomass exceeds a certain threshold ($[PHY_0]$). No specific preference for grazing on particular phytoplankton species is considered among zooplankton species. Instead, the phytoplankton biomass grazed by the i^{th} species of zooplankton is divided proportionally among each species of phytoplankton (Eq. (22)). The growth rate of zooplankton is considered proportional to grazing rate using a growth yield factor (Eq. (28)).

$$b_{zoo_i} = b_{max20,zoo_i} f(T)_{zoo_i} \frac{(\sum_j^{NS} [PHY_j] - [PHY_0]_{zoo_i})}{(\sum_j^{NS} [PHY_j] - [PHY_0]_{zoo_i}) + K_{phy,zoo_i}} \quad (27)$$

$$\mu_{zoo_i} = Y_{zoo_i} b_{zoo_i} \quad (28)$$

340 With b_{zoo_i} : Effective grazing rate of the i^{th} zooplankton species, [h^{-1}]

b_{max20,zoo_i} : Maximal grazing rate of the i^{th} zooplankton species at 20 °C, [h^{-1}]

$f(T)_{zoo_i}$: Water temperature weight of the i^{th} zooplankton species at T °C defined like the equation (2), [-]

$\sum_j^{NS} [PHY_j]$: Total phytoplankton biomass with NS the number of phytoplankton species grazed by zooplankton, [$mgC L^{-1}$]

$[PHY_0]_{zoo_i}$: Phytoplankton biomass threshold above which grazing takes place for the i^{th} zooplankton species, [$mgC L^{-1}$]

345 K_{phy,zoo_i} : Half-saturation constant for phytoplankton biomass of the i^{th} zooplankton species, [$mgC L^{-1}$]

μ_{zoo_i} : Growth rate of the i^{th} zooplankton species, [h^{-1}]

Y_{zoo_i} : Growth yield of the i^{th} zooplankton species, [-]

2.4.2 Respiration and Mortality

Grazed phytoplankton not used for zooplankton growth is respired (Fig. 4). The rate of respiration is then obtained by (1 –
350 Y_{zoo}) $\times b_{zoo}$. The mortality of zooplankton is simulated by a first order kinetics ($k_{d20,zoo}$).

$$r_{zoo_i} = (1 - Y_{zoo_i}) \times b_{zoo_i} \quad (29)$$

$$\frac{d[ZOO_i]}{dt} = (Y_{zoo_i} b_{zoo_i} - k_{d20,zoo_i} f(T)_{zoo_i} - k_{sink,zoo_i}) [ZOO_i] \quad (30)$$

With r_{zoo_i} : Respiration rate of the i^{th} zooplankton species, [h^{-1}]

Y_{zoo_i} : Growth yield of the i^{th} zooplankton species, [-]

355 b_{zoo_i} : Effective grazing rate of the i^{th} zooplankton species (Eq. (27)), [h^{-1}]

k_{d20,zoo_i} : Mortality rate of the i^{th} zooplankton species at 20 °C, [h^{-1}]

$f(T)_{zoo_i}$: Water temperature weight of the i^{th} zooplankton species at T °C defined like the equation (2), [-]

k_{sink,zoo_i} : Sinking rate of the i^{th} zooplankton species, [h^{-1}]

$[ZOO_i]$: Biomass concentration of the i^{th} zooplankton species, [$mgC L^{-1}$]

360 2.5 Nutrient cycling

As shown above, several processes related to nutrients are taken into account: uptake by phytoplankton, mineralization, nitrification, denitrification (Fig. 5, and Fig. 6).

2.5.1 Uptake of nutrients (N, P, Si) by phytoplankton

The Redfield-Conley stoichiometry (C:N:P:Si = 106:16:1:42, (Redfield et al., 1963; Conley et al., 1989) is used to determine
365 the composition of carbon, nitrogen, and phosphorus in organic matter. Constant C/N, C/P and C/Si mass ratios are considered to calculate the uptake of nutrient associated to phytoplankton growth.

$$\frac{d[uptN]}{dt} = \sum_i \frac{(\mu_{F_i} + e_{phy_i}) [F_i]}{C/N} \quad (31)$$

$$uptNH_4^+ = \min\left([NH_4^+], uptN \left(\frac{[NH_4^+]}{[NH_4^+] + [NO_3^-]}\right)^{0.025}\right) \quad (32)$$

$$uptNO_3^- = uptN - uptNH_4^+ \quad (33)$$

$$370 \frac{d[uptP]}{dt} = \sum_i \frac{(\mu_{F_i} + e_{phy_i}) [F_i]}{C/P} \quad (34)$$

$$\frac{d[uptSi]}{dt} = \frac{\mu_{F,dia} [F_{dia}]}{C/Si} \quad (35)$$

- With μ_{F_i} : Effective growth rate of the i^{th} phytoplankton species (Eq. (16)), [h^{-1}]
- e_{phy_i} : Excretion rate of the i^{th} phytoplankton species (Eq. (19)), [h^{-1}]
- $[F_i]$: Functional macromolecules concentration of the i^{th} phytoplankton species, [$mgC L^{-1}$]
- 375 $[NH_4^+]$ and $[NO_3^-]$: Concentrations of ammonium and nitrate, [$mgN L^{-1}$]
- $uptN$: Uptake of nitrogen for phytoplankton growth, [$mgN L^{-1}$]
- $uptNH_4^+$: Uptake of NH_4^+ for phytoplankton growth, [$mgN L^{-1}$]
- $uptNO_3^-$: Uptake of NO_3^- for phytoplankton growth, [$mgN L^{-1}$]
- $uptP$: Uptake of phosphorus for phytoplankton growth, [$mgP L^{-1}$]
- 380 C/N : Carbon to nitrogen mass ratio, [mgC/mgN]
- C/P : Carbon to phosphorus mass ratio, [mgC/mgP]
- C/Si : Carbon to silica mass ratio, [$mgC/mgSi$]
- $uptSi$: Uptake of silica for diatoms growth, [$mgSi L^{-1}$]
- $\mu_{F, dia}$: Effective growth rate of Diatoms, [h^{-1}]
- 385 $[F_{dia}]$: Functional macromolecules (**F**) concentration of Diatoms, [$mgC L^{-1}$]

2.5.2 Release of nutrients by mineralization

The mineralization of organic matter by heterotrophic bacteria and zooplankton is achieved by its oxidation through respiration (Fig. 5). The process consumes organic matter and releases nitrogen and phosphorus from the fraction that is not assimilated for growth of heterotrophic bacteria and zooplankton.

$$390 \quad respHB = \sum_i (1 - Y_{hb_i}) b_{hb_i} [HB_i] \quad (36)$$

$$respZOO = \sum_j (1 - Y_{zoo_j}) b_{zoo_j} [ZOO_j] \quad (37)$$

$$relN = \frac{respHB}{C/N} + \frac{respZOO}{C/N} \quad (38)$$

$$relP = \frac{respHB}{C/P} + \frac{respZOO}{C/P} \quad (39)$$

- With $respHB$: Respiration of heterotrophic bacteria species, [$mgC L^{-1} h^{-1}$]
- 395 Y_{hb_i} : Growth yield of the i^{th} heterotrophic bacteria species, [-]
- b_{hb_i} : Effective rate of substrate uptake by the i^{th} heterotrophic bacteria species (Eq. (1)), [h^{-1}]
- $[HB_i]$: Concentration of the i^{th} heterotrophic bacteria species, [$mgC L^{-1}$]
- $respZOO$: Respiration of zooplankton species, [$mgC L^{-1} h^{-1}$]
- Y_{zoo_j} : Growth yield of the j^{th} zooplankton species, [-]
- 400 b_{zoo_j} : Effective grazing rate of the j^{th} zooplankton species (Eq. (27)), [h^{-1}]
- $[ZOO_j]$: Concentration of the j^{th} zooplankton species, [$mgC L^{-1}$]
- $relN$: Release of nitrogen, [$mgN L^{-1} h^{-1}$]

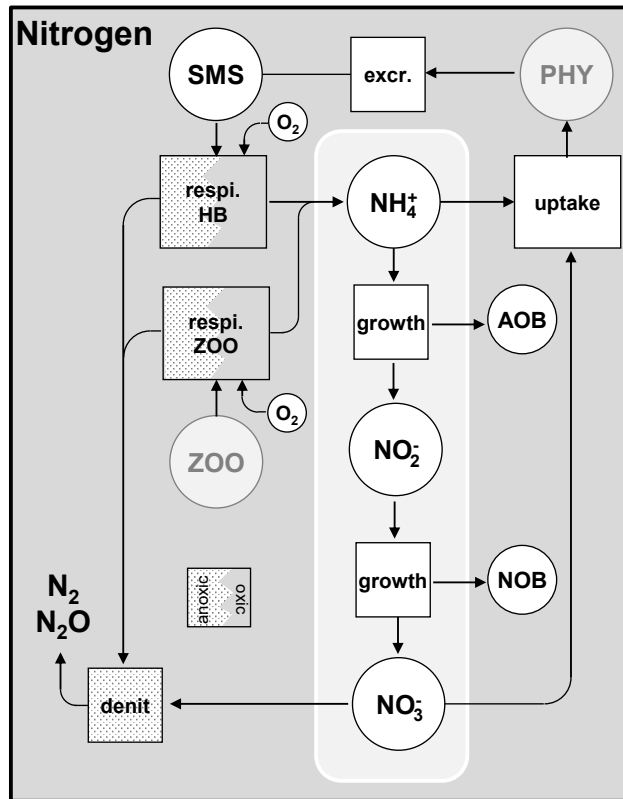


Figure 5. Cycling of nitrogen. PHY: phytoplankton species; HB: heterotrophic bacteria; ZOO: zooplankton species; AOB: ammonia-oxidizing bacteria; NOB: Nitrite-oxidizing bacteria; respi.: respiration; excr.: excretion; denit: denitrification

C/N : Carbon to nitrogen mass ratio, [mgC/mgN]

$relP$: Release of phosphorus, [mgP L⁻¹ h⁻¹]

405 C/P : Carbon to phosphorus mass ratio, [mgC/mgP]

2.5.3 Nitrification and denitrification

As mentioned in the section 2.2, the nitrification process (Fig. 2 and Fig. 5) is related to the growth of AOB (ammonia-oxidizing bacteria) and NOB (nitrite-oxidizing bacteria). Growth yields (Y_{aob_i} and Y_{nob_j}) are used to describe the amount of nitrogen consumed by nitrifying bacteria (Eq. (40) and (41)). The denitrification occurs when dissolved oxygen is not present
410 in sufficient quantity (Fig. 5).

$$nitr_{aob} = \sum_i \frac{\mu_{aob_i}}{Y_{aob_i}} [AOB_i] \quad (40)$$

$$nitr_{nob} = \sum_j \frac{\mu_{nob_j}}{Y_{nob_j}} [NOB_j] \quad (41)$$

With μ_{aob_i} and μ_{nob_j} : Effective growth rates of the i^{th} AOB species (Eq. (7)) and the j^{th} NOB species (Eq. (8)), [h^{-1}]

Y_{aob_i} and Y_{nob_j} : Growth yields of the i^{th} AOB species and the j^{th} NOB species, [mgC/mgN]

415 $nitr_{aob}$: Nitrification $NH_4^+ + \frac{3}{2}O_2 \rightarrow NO_2^- + H_2O + 2H^+$, [mgN L⁻¹ h⁻¹]

$nitr_{nob}$: Nitrification $NO_2^- + \frac{1}{2}O_2 \rightarrow NO_3^-$, [mgN L⁻¹ h⁻¹]

$[AOB_i]$ and $[NOB_j]$: Biomass concentrations of the i^{th} AOB species and the j^{th} NOB species, [mgC L⁻¹]

The budgets of NO_3^- , NH_4^+ and NO_2^- can then be established.

$$420 \quad \frac{d[NO_3^-]}{dt} = -denit + nitr_{nob} - \frac{uptNO_3^-}{dt} \quad (42)$$

$$\frac{d[NH_4^+]}{dt} = relN - nitr_{aob} - \frac{uptNH_4^+}{dt} \quad (43)$$

$$\frac{d[NO_2^-]}{dt} = nitr_{aob} - nitr_{nob} \quad (44)$$

With $denit$: Denitrification, [mgN L⁻¹ h⁻¹]

$nitr_{nob}$: Nitrification by NOB (Eq. (41)), [mgN L⁻¹ h⁻¹]

425 $nitr_{aob}$: Nitrification by AOB (Eq. (40)), [mgN L⁻¹ h⁻¹]

$\frac{uptNO_3^-}{dt}$: Uptake of NO_3^- by phytoplankton growth (Eq. (33)), [mgN L⁻¹ h⁻¹]

$relN$: Release of nitrogen by respiration of heterotrophic bacteria and zooplankton (Eq. (38)), [mgN L⁻¹ h⁻¹]

$\frac{uptNH_4^+}{dt}$: Uptake of NH_4^+ by phytoplankton growth (Eq. (32)), [mgN L⁻¹ h⁻¹]

2.5.4 Phosphate adsorption desorption

430 Orthophosphate (PO_4^{3-}) is released by mineralization and uptaken by phytoplankton exactly as inorganic nitrogen (Fig. 6). Once released in the water column, however, orthophosphates are subject to a process of adsorption-desorption on mineral suspended solids (MSS) to form PIP (particulate inorganic phosphorus). In addition, the impact of sediment dynamics on P fluxes should be considered in the future work in unified RIVE. Vilmin et al. (2015a) showed that P fluxes are mainly driven by hydrological conditions and sediment-related processes in Seine river system.

435 The process is represented according to an instantaneous hyperbolic equilibrium relationship of the form:

$$\frac{[PIP]}{[MSS]} = P_{ac} \times \frac{[PO_4^{3-}]}{[PO_4^{3-}] + K_{ps}} \quad (45)$$

With $\frac{[PIP]}{[MSS]}$: Inorganic P content of MSS, [mgP mgMSS⁻¹]

$[PIP]$ and $[MSS]$: Concentrations of PIP and MSS, [mgP L⁻¹] and [mgMSS⁻¹]

P_{ac} : Maximum adsorption capacity of MSS, [mgP mgMSS⁻¹]

440 $[PO_4^{3-}]$: Concentration of orthophosphate, [mgP L⁻¹]

K_{ps} : Half saturation adsorption constant, [mgP L⁻¹]

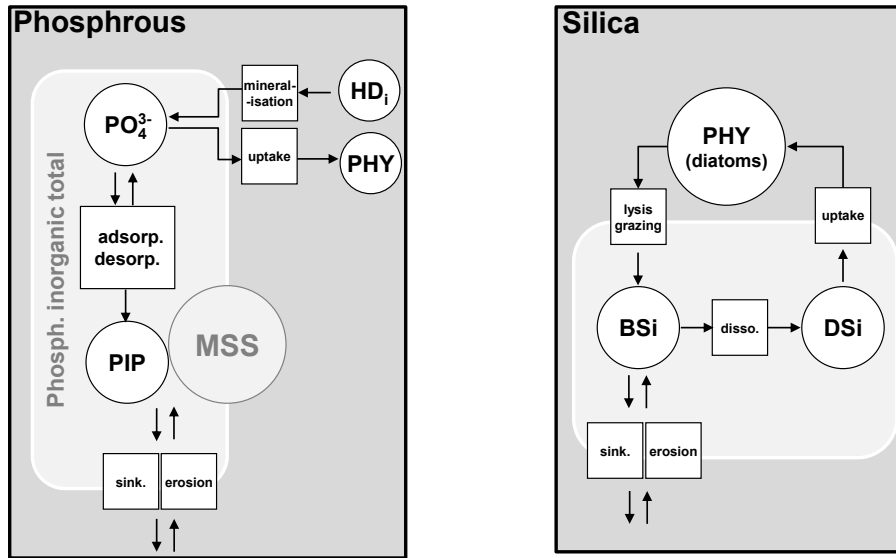


Figure 6. Phosphorus and silica dynamics. HD: dissolved high weight polymer; PHY: phytoplankton; PIP: particulate inorganic phosphorus; MSS: mineral suspended solids; BSi: biogenic silica; DSi: dissolved silica; adsorp.: adsorption; desorp.: desorption; sink.: sinking; disso. dissolution

Considering this equilibrium instantaneously reached implies that a relationship exists between the variables PIP, MSS, PO_4^{3-} and TIP (total inorganic phosphorus):

$$[TIP] = [PO_4^{3-}] + [PIP] \quad (46)$$

445 This equilibrium relationship can be written:

$$[PO_4^{3-}] = \frac{([TIP] - P_{ac} \times [MSS] - K_{ps}) + \sqrt{(-[TIP] + P_{ac} \times [MSS] + K_{ps})^2 + 4 \times [TIP] \times K_{ps}}}{2} \quad (47)$$

With $[PO_4^{3-}]$: Concentration of orthophosphate, $[mgP L^{-1}]$

$[TIP]$ and $[MSS]$: Concentrations of TIP and MSS, $[mgP L^{-1}]$ and $[mgMSS^{-1}]$

P_{ac} : Maximal adsorption capacity of MSS, $[mgP mgMSS^{-1}]$

450 K_{ps} : Half saturation adsorption constant, $[mgP L^{-1}]$

2.5.5 Silica dynamics

Dissolved silica (DSi) is produced by the dissolution of dead frustules of diatoms (designated as biogenic silica, BSi). The rock weathering contributes also dissolved silica while it is considered as null in unified RIVE v1.0. DSi is uptaken by the growth of diatoms (Fig. 6). Biogenic silica is produced by the lysis and grazing of diatoms, settles down and dissolves according to a

455 first order kinetics, dependent on water temperature (Rickert et al., 2002):

$$BSi_{diss.} = Kb_{Si} \times [BSi] \quad (48)$$

$$Kb_{Si} = Kb_{Si20} \times ftp_{Si}(T) \quad (49)$$

$$ftp_{Si}(T) = \exp\left(\frac{60000}{8.314} \times \left(\frac{1}{275} - \frac{1}{273 + T}\right)\right) \quad (50)$$

With Kb_{Si20} : Dissolution rate of biogenic silica at 20 °C, [h^{-1}]

460 $[BSi]$: Concentration of biogenic silica, [$mgSi L^{-1}$]

T : Water temperature, [$^{\circ}C$]

2.6 Dissolved oxygen

Dissolved oxygen is especially influenced by photosynthesis and respiration. The reaeration at the water-air interface is also included in unified RIVE v1.0 model. The sediment dynamics are important for sediment oxygen demand (not shown here).

465 Vilmin et al. (2016) showed that benthic respiration accounts for one third of the total Seine river respiration. Relevant efforts about sediment dynamics need to be made in future work, which is not the focus of this study. An oxygen budget can then be established (Eq. (51)).

$$\frac{d[O_2]}{dt} = rea + \frac{32}{12} \left(\sum_i (p_{phy_i} - r_{phy_i}) [F_i] - resp_{HB} - \sum_j r_{zoo_j} [ZOO_j] \right) - \frac{32}{14} \left(\frac{3}{2} nitr_{aob} + \frac{1}{2} nitr_{nob} \right) \quad (51)$$

$$rea = \frac{k_{rea}}{depth} ([O_2]_{sat} - [O_2]) \quad (52)$$

470 With, k_{rea} : Reaeration coefficient, [$m h^{-1}$]

$depth$: Water height, [m]

$[O_2]_{sat}$: Saturated concentration of dissolved oxygen in water, [$mgO_2 L^{-1}$]

$[O_2]$: Concentration of dissolved oxygen in water, [$mgO_2 L^{-1}$]

$\frac{32}{12}$: Molar mass ratio between dissolved oxygen and carbon, [mgO_2/mgC]

475 p_{phy_i} : Photosynthesis rate of the i^{th} phytoplankton species (Eq. (14)), [h^{-1}]

r_{phy_i} : Respiration rate of the i^{th} phytoplankton species (Eq. (18)), [h^{-1}]

$[F_i]$: Functional biomass concentration of the i^{th} phytoplankton species, [$mgC L^{-1}$]

$resp_{HB}$: Respiration of all heterotrophic bacteria species (Eq. (36)), [$mgC L^{-1} h^{-1}$]

r_{zoo_j} : Respiration rate of the j^{th} zooplankton species (Eq. (29)), [h^{-1}]

480 $[ZOO_j]$: Biomass concentration of the j^{th} zooplankton species, [$mgC L^{-1}$]

$\frac{32}{14}$: Molar mass ratio between dissolved oxygen and nitrogen, [mgO_2/mgN]

$nitr_{aob}$: Nitrification to produce nitrite by oxidizing NH_4^+ (Eq. (40), with $\frac{3}{2}$ the stoichiometric coefficient), [$mgN L^{-1} h^{-1}$]

$nitr_{nob}$: Nitrification to produce nitrate by oxidizing NO_2^- (Eq. (41), with $\frac{1}{2}$ the stoichiometric coefficient), [$mgN L^{-1} h^{-1}$]

2.7 Inorganic carbon

485 An inorganic carbon module is implemented in unified RIVE v1.0. The carbonate system is described by a set of equations (named the CO₂ module) based on a previous representation provided by Gypens et al. (2004) and adapted for freshwater environments (Marescaux et al., 2020). In this module, four state variables are defined: dissolved inorganic carbon (DIC), total alkalinity (TA), acidity (pH) and aqueous carbon dioxide (CO₂(aq)).

2.7.1 CO₂ flux at air-water interface

490 The DIC is defined as the sum of three dissolved carbonate species:

$$[\text{DIC}] = [\text{H}_2\text{CO}_3] + [\text{HCO}_3^-] + [\text{CO}_3^{2-}] \quad (53)$$

The calculation of pH is derived from Culberson (1980) using TA and DIC. Then the aqueous carbon dioxide (CO₂ (aq)) is derived from the carbonate chemical equilibrium using DIC and pH (Marescaux et al., 2020; Yan et al., 2022a).

$$[\text{CO}_2(\text{aq})] = \frac{[\text{DIC}] \frac{[\text{H}^+]}{K_1}}{\left(1 + \frac{[\text{H}^+]}{K_1} + \frac{K_2}{[\text{H}^+]}\right)} \quad (54)$$

495 With K_1 , K_2 : Equilibrium constants of carbonate equilibrium reactions (Stumm and Morgan, 1996), [mol L⁻¹]

$[\text{H}^+]$: Concentration of hydrogen ions with $\text{pH} = -\log([\text{H}^+])$, [mol L⁻¹]

$[\text{DIC}]$: Concentration of dissolved inorganic carbon, [mgC L⁻¹]

The flux of CO₂ at water-air interface (F_{CO_2} , gC m⁻² h⁻¹) is calculated based on Fick's first law (Fick, 1855) with a gas transfer velocity of CO₂ (k_{CO_2}).

$$500 \quad F_{\text{CO}_2} = k_{\text{CO}_2}([\text{CO}_2(\text{sat})] - [\text{CO}_2(\text{aq})]) \quad (55)$$

With k_{CO_2} : Gas transfer velocity of CO₂, [m h⁻¹]

$[\text{CO}_2(\text{sat})]$: Solubility of CO₂ in water, calculated based on Henry's law (Weiss, 1974), [mgC L⁻¹]

$[\text{CO}_2(\text{aq})]$: Aqueous carbon dioxide concentration, [mgC L⁻¹]

The gas transfer velocity of CO₂ (k_{CO_2}) depends on water temperature and k_{600} (gas transfer velocity of CO₂ for a Schmidt number of 600, corresponding to a temperature of 20 °C in freshwater). According to Wilke and Chang (1955), Jähne et al. (1987) and Wanninkhof (1992), the gas transfer velocity of CO₂ (k_{CO_2}) at water temperature T (°C) can be calculated as:

$$k_{\text{CO}_2} = k_{600} \sqrt{\frac{600}{Sc_{\text{CO}_2}(T)}} \quad (56)$$

where k_{600} (m h⁻¹) is the gas transfer velocity of CO₂ for a Schmidt number of 600, and $Sc_{\text{CO}_2}(T)$ is the Schmidt number (dimensionless) calculated with the water temperature in Celsius degree (°C). The $Sc_{\text{CO}_2}(T)$ can be determined as,

$$510 \quad Sc_{\text{CO}_2}(T) = 1911.1 - 118.11T + 3.4527T^2 - 0.04132T^3 \quad (57)$$

2.7.2 Budgets of TA and DIC

The processes such as respiration, photosynthesis, nitrification, denitrification and input flows affect TA and DIC. The unified RIVE v1.0 considers these processes explicitly.

$$515 \quad \frac{dT A}{dt} = \left[\left(\frac{14}{106} \times \frac{(respPHY + respHB + respZOO)}{12} \right) + \frac{(denit - 2 \cdot nitr_{aob})}{14} \right. \\ \left. + \left(\frac{17}{106} \times \frac{uptNO_3^-}{uptN} - \frac{15}{106} \times \frac{uptNH_4^+}{uptN} \right) \times \frac{\sum(\mu_{F_i} + e_{phy_i})[F_i]}{12} \right] \times 1000 + TA_{Net_Input} \quad (58)$$

$$\frac{dDIC}{dt} = (respPHY + respHB + respZoo) + denit \times \frac{12}{14} \times \frac{5}{4} \\ - \sum p_{phy_i} [F_i] + \frac{FCO_2}{depth} + DIC_{Net_Input} \quad (59)$$

where TA_{Net_input} ($\mu\text{mol L}^{-1} \text{h}^{-1}$) and DIC_{Net_input} ($\text{mgC L}^{-1} \text{h}^{-1}$) are the net input fluxes. The respiration of all phytoplankton, bacteria, zooplankton species ($respPHY$, $respHB$, $respZOO$, $\text{mgC L}^{-1} \text{h}^{-1}$) transform organic carbon to CO_2 by full oxidation. The denitrification ($denit$, $\text{mgN L}^{-1} \text{h}^{-1}$) is considered also in the calculation of TA and DIC. FCO_2 ($\text{gC m}^{-2} \text{h}^{-1}$) is the CO_2 flux at air-water interface. $depth$ is the water depth (m). $\frac{14}{106}$, $\frac{17}{106}$, $\frac{15}{106}$, $\frac{5}{4}$ are the stoichiometry coefficients of biogeochemical processes (Marescaux et al., 2020).

2.8 Kinetic parameters in unified RIVE model

120 parameters are used to describe the aforementioned processes considering three phytoplankton species and two heterotrophic bacteria species. Some of them depend on water temperature and are calculated with a water temperature function (Eq. (2)). Their definitions and reference values are provided in appendix B.

3 Results

3.1 Digital implementation with Python 3 (pyRIVE 1.0) or ANSI C (C-RIVE 0.32)

The above unified governing equations are implemented in Python 3 to create pyRIVE 1.0 (<https://doi.org/10.48579/PRO/Z9ACPI>; Thieu et al. (2023)) and in ANSI C to create C-RIVE 0.32 (<https://doi.org/10.5281/zenodo.7849609>; Wang et al. (2023b)), respectively. A Jupyter Notebook is used for pedagogical exercises with pyRIVE 1.0, while C-RIVE 0.32 needs to be compiled with gcc under a Linux or a MAC OS operating system. In addition, the user interface of C-RIVE 0.32 uses its own parser based on flex and bison, which allows the software to read ASCII files.

In practice, the number of living species is predefined in pyRIVE 1.0 while we have the ability to define as many species as desired in C-RIVE 0.32 (Tab. 1). For instance, three communities of phytoplankton (DIA: Diatoms; GRA: Green algae; CYA: Cyanobacteria), two populations of heterotrophic bacteria distinct by their growth rate and size (small one SHB and large one LHB; Garnier et al. (1992a)) and two zooplankton communities (ZOR: Rotifer and ZOC: MicroCrustaceans; Billen et al. (1994); Garnier et al. (1995, 2000)) are predefined in pyRIVE 1.0.

In addition, the TIP (total inorganic phosphorus) is considered as a state variable in pyRIVE 1.0. PO_4^{3-} and PIP are derived from it according to Eq. (46) and Eq.(47). TIP is subject to release by heterotrophic bacteria and zooplankton respiration (Eq. (39)), uptake by phytoplankton and settling of PIP together with MSS. However, the PO_4^{3-} is treated as a state variable and released by respiration (Eq. (39)) in C-RIVE 0.32 and only PIP (particulate inorganic phosphorus) is derived from the equation (45).

Table 1. Number of living species defined in pyRIVE 1.0 and C-RIVE 0.32 which implement the unified RIVE v1.0

| Species | PHY | HB | AOB | NOB | ZOO |
|-------------|--------------|--------------|--------------|--------------|--------------|
| pyRIVE 1.0 | 3 | 2 | 1 | 1 | 2 |
| C-RIVE 0.32 | User-defined | User-defined | User-defined | User-defined | User-defined |

3.2 Modeling of the organic matter degradation by unified RIVE v1.0 (HSB model)

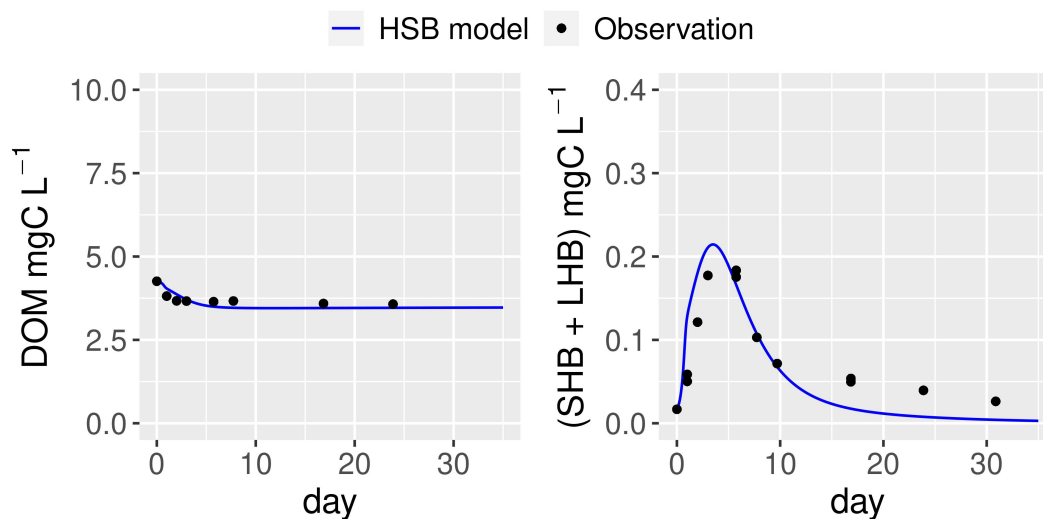


Figure 7. Simulation of the dynamics of heterotrophic bacteria in a filtered and reinoculated sample of the drainage pond water (Seine basin, France) in February 2021 (Garnier et al., 2021) by HSB model (unified RIVE v1.0). DOM: Dissolved organic matter; SHB: Small heterotrophic bacteria.

The ability of the HSB model (Fig. 1) to simulate organic matter degradation has been verified by modelling two batch experiments conducted by Garnier et al. (2021). Two water samples were used in the study. One sample was obtained from a drainage pond in the Seine basin, France, in February 2021 (Fig. 7). The other sample was collected from an urban sewage collector in Rosny-sur-Seine, France, in February 2021 (Fig. 8). These samples were incubated in the dark at a temperature

of 21°C for a period of 45 days, during which aerobic bacteria consumed organic matter (Servais et al., 1995). Only DOM
 550 and bacterial biomass are measured during batch experiments and then used to show validation. The HSB model is able to
 effectively reproduce the concentrations of dissolved organic matter and bacterial biomass with a trial-error adjustment of its
 parameter values (Fig. 7 and 8). The parameter values are kept the same for both water samples.

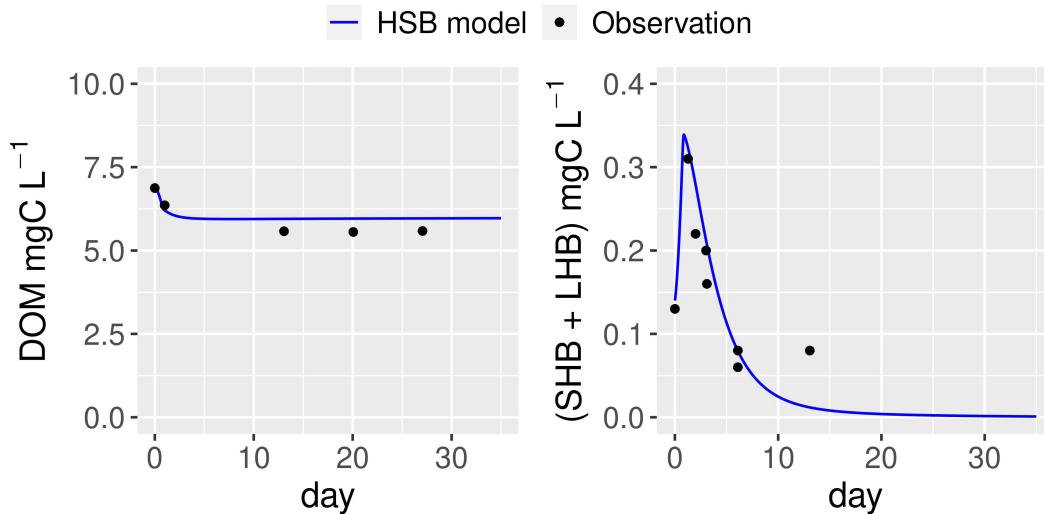


Figure 8. Simulation of the dynamics of heterotrophic bacteria in a filtered and reinoculated sample of the urban sewage water (Rosny-sur-Seine, France) in February 2021 (Garnier et al., 2021) by HSB model (unified RIVE v1.0). DOM: Dissolved organic matter; SHB: Small heterotrophic bacteria; LHB: Large heterotrophic bacteria

3.3 A river stretch simulated with unified RIVE v1.0: pyRIVE 1.0 vs. C-RIVE 0.32

A river stretch with a Strahler order of 8 (Fig. 9) is designed to compare the results simulated by two versions of unified RIVE
 555 v1.0 implemented in pyRIVE 1.0 and C-RIVE 0.32. The case study allows us to compare the two versions of unified RIVE
 v1.0 under transient contrasting conditions i) between species communities, and ii) temporally for each species community.

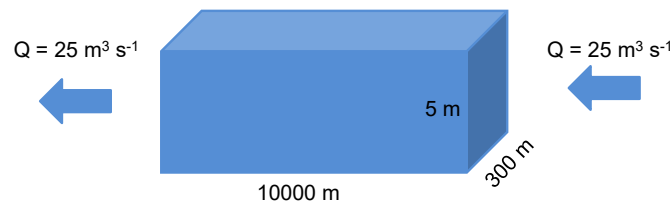


Figure 9. Geometric and hydraulic description of a river stretch

3.3.1 River stretch morphology and hydraulic conditions

The stretch measures 10000 meters long and 300 meters width. To simplify the boundary conditions, the upstream inflow and downstream outflow are fixed at $25 \text{ m}^3 \text{ s}^{-1}$ which corresponds to a residence time of 7 days. The water height is fixed at 5
560 meters.

3.3.2 Simulation settings and evaluation strategy

The concentrations of all water quality variables of inflow are defined as their initial concentrations in the stretch and remain constant during the simulation (Tab. 2). Since this paper focuses on the conceptualization of the unified RIVE v1.0 in water column, no exchange between benthic layer and water column are considered. The time step of the simulation is 6 min and a
565 simulation period of 365 days is considered. To compare the results of the two digital implementations of unified RIVE v1.0, daily concentrations at 00:00 are plotted. Three statistical criteria (PBIAS: Percent Bias (%); MAD: Mean Absolute Difference; MaAD: Maximum Absolute Difference) are calculated to evaluate the similarity of the two set of results. The closer the criteria are to 0, the more similar are the concentrations simulated by the two softwares (pyRIVE 1.0 and C-RIVE 0.32).

$$PBIAS = 100 \frac{\sum_{i=1}^{i=N} (C_i - Py_i)}{\sum_{i=1}^{i=N}} \quad (60)$$

$$570 \quad MAD = \frac{\sum_{i=1}^{i=N} |C_i - Py_i|}{N} \quad (61)$$

$$MaAD = \max(|C_i - Py_i|) \quad (62)$$

Where C_i represent the concentrations simulated by C-RIVE 0.32 (in ANSI C) and Py_i those simulated by pyRIVE 1.0 (in Python 3). N is the number of values.

3.3.3 Simulated concentrations of water quality variables

575 The concentrations simulated by pyRIVE 1.0 and C-RIVE 0.32 are very similar (and superimposed) for all water quality variables (Fig. 10). A maximum absolute difference (MaAD) of $0.0307 \text{ mgO}_2 \text{ L}^{-1}$, which is relatively low, is obtained for dissolved oxygen concentration. The mean absolute difference (MAD) for dissolved oxygen concentration is $0.00678 \text{ mgO}_2 \text{ L}^{-1}$ (Tab. 3) and the corresponding percent bias (PBIAS) is 0%. The MaAD of $0.0307 \text{ mgO}_2 \text{ L}^{-1}$ for dissolved oxygen is cause of the depletion of CYA S (small precursors S of cyanobacteria, Fig. 3) at the beginning of the simulation (not shown here).
580 To correct this depletion of CYA S, the growth of functional macromolecules (CYA F) is reduced according to the availability of CYA S in C-RIVE 0.32. That's why the simulated concentrations of CYA (cyanobacteria) depict a MaAD of $0.0321 \text{ mgC L}^{-1}$ between pyRIVE 1.0 and C-RIVE 0.32. Due to this auto-correction in C-RIVE 0.32, the simulated concentrations of CYA by C-RIVE 0.32 are slightly smaller than those simulated by pyRIVE 1.0 (PBIAS = -1.2%). The values of PBIAS indicate also the similarity between the concentrations simulated by pyRIVE 1.0 and C-RIVE 0.32. Except for CYA, the discrepancies
585 of other variables are extremely low compared to their concentrations (PBIAS $\leq 0.6\%$). More than half of simulated variables have a PBIAS of 0%.

Table 2. Initial concentrations and boundary conditions

| Species | Description | C_{init} | $C_{boundary}$ | Unit |
|----------------------|--|----------------------|----------------------|-------------------------------------|
| SHB | Small heterotrophic bacteria | 0.005 | 0.005 | [mgC L ⁻¹] |
| LHB | Large heterotrophic bacteria | 0.004 | 0.004 | [mgC L ⁻¹] |
| AOB | Ammonia-oxidizing bacteria | 0.001 | 0.001 | [mgC L ⁻¹] |
| NOB | Nitrite-oxidizing bacteria | 0.0002 | 0.0002 | [mgC L ⁻¹] |
| DIA | Diatoms | 0.447 | 0.447 | [mgC L ⁻¹] |
| GRA | Green algae | 0.539 | 0.539 | [mgC L ⁻¹] |
| CYA | Cyanobacteria | 0.662 | 0.662 | [mgC L ⁻¹] |
| ZOR | Rotifer | $9.33 \cdot 10^{-5}$ | $9.33 \cdot 10^{-5}$ | [mgC L ⁻¹] |
| ZOC | MicroCrustaceans | $9.33 \cdot 10^{-6}$ | $9.33 \cdot 10^{-6}$ | [mgC L ⁻¹] |
| SMS | Small monomeric substrate | 0.036 | 0.036 | [mgC L ⁻¹] |
| DOM ₁ | Rapidly biodegradable dissolved organic matter | 0.022 | 0.022 | [mgC L ⁻¹] |
| DOM ₂ | Slowly biodegradable dissolved organic matter | 0.174 | 0.174 | [mgC L ⁻¹] |
| DOM ₃ | Dissolved refractory organic matter | 1.625 | 1.625 | [mgC L ⁻¹] |
| POM ₁ | Rapidly biodegradable particulate organic matter | 0.005 | 0.005 | [mgC L ⁻¹] |
| POM ₂ | Slowly biodegradable particulate organic matter | 0.021 | 0.021 | [mgC L ⁻¹] |
| POM ₃ | Particulate refractory organic matter | 0.107 | 0.107 | [mgC L ⁻¹] |
| NH ₄ | Ammonium | 1.5 | 1.5 | [mgN L ⁻¹] |
| NO ₂ | Nitrite | 0.016 | 0.016 | [mgN L ⁻¹] |
| NO ₃ | Nitrate | 0.941 | 0.941 | [mgN L ⁻¹] |
| TIP | Total inorganic phosphorus | 0.2 | 0.2 | [mgP L ⁻¹] |
| DSi | Dissolved silica | 3.090 | 3.090 | [mgSi L ⁻¹] |
| MSS | Mineral suspended solids | 2.611 | 2.611 | [mg L ⁻¹] |
| OXY | Dissolved oxygen | 9.446 | 9.446 | [mgO ₂ L ⁻¹] |
| TA | Total alkalinity | 5291 | 5291 | [μmol L ⁻¹] |
| DIC | Dissolved inorganic carbon | 62.728 | 62.728 | [mgC L ⁻¹] |
| CO ₂ (aq) | Aqueous carbon dioxide | 0.343 | 0.343 | [mgC L ⁻¹] |
| pH | Acidity | 8.659 | 8.695 | [-] |

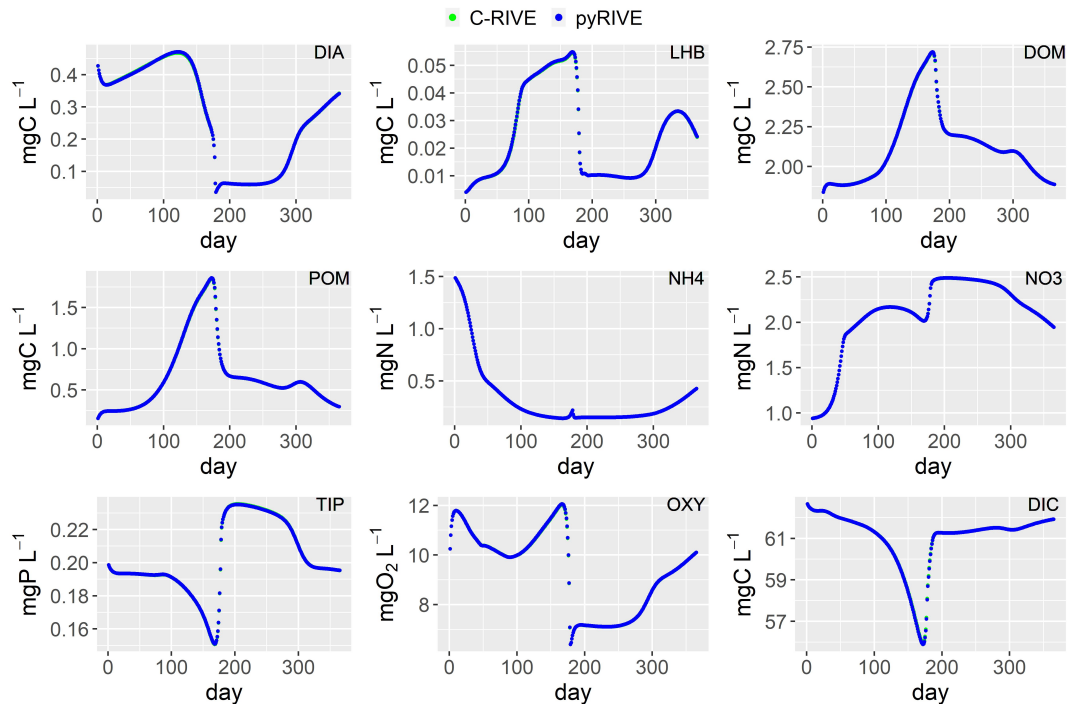


Figure 10. Simulated concentrations of main species by pyRIVE 1.0 and C-RIVE 0.32. See table 2 for their definitions

4 Discussion

The results show the ability of the unified RIVE v1.0 to simulate correctly the organic matter degradation and the similarity of its two digital implementations (pyRIVE 1.0 and C-RIVE 0.32). Here, we discuss the biogeochemical cycling simulated by unified RIVE v1.0 in water column (Section 4.1), the model limitations, the future developments (Section 4.3) and its benefits for scientific community (Section 4.4).

4.1 Biogeochemical cycling in water column simulated by unified RIVE v1.0

The unified RIVE v1.0 simulates the dynamics of microorganisms involving biogeochemical cycling, although the boundary conditions are defined as constant for modeling a river stretch (Fig. 9). Here we interpret the dynamics of diatoms (DIA) and large heterotrophic bacteria (LHB). For this purpose, the budget fluxes of DIA and LHB are calculated.

The decreasing of DIA biomass from day 1 to day 15 is related to the low water temperature and low active irradiance which limit its photosynthesis (Fig. 10, Fig. 12). The optimal temperature for the growth of DIA is 21 °C while the water temperature is lower than 3 °C (Fig. 12). The low photosynthesis rate leads to a negative net production (Fig. 11, green line), which is the difference between the fluxes of photosynthesis and the combined fluxes of respiration, mortality, and excretion. During this period, while the input factors play a positive role, the net change of DIA is still negative (Fig. 11, black line). Over

Table 3. Statistical criteria for comparing the simulated variables by pyRIVE 1.0 and C-RIVE 0.32 which implement the unified RIVE v1.0. PBIAS: Percent Bias [%]; MAD: Mean Absolute Difference; MaAD: Maximum Absolute Difference. The units of MAD and MaAD are either [mgC L⁻¹] or [mgN L⁻¹] or [mgP L⁻¹] or [mgSi L⁻¹] or [μ mol L⁻¹].

| Species | PBIAS | MAD | MaAD | Species | PBIAS | MAD | MaAD |
|------------------|-------|----------------------|----------------------|----------------------|-------|----------------------|----------------------|
| SHB | -0.4 | $2.07 \cdot 10^{-5}$ | $1.40 \cdot 10^{-4}$ | LHB | -0.4 | $1.10 \cdot 10^{-4}$ | $4.27 \cdot 10^{-4}$ |
| AOB | 0 | $1.78 \cdot 10^{-5}$ | $6.95 \cdot 10^{-5}$ | NOB | 0 | $4.85 \cdot 10^{-6}$ | $1.98 \cdot 10^{-5}$ |
| DIA | -0.1 | $1.07 \cdot 10^{-3}$ | $3.63 \cdot 10^{-3}$ | GRA | -0.1 | $4.98 \cdot 10^{-4}$ | $1.87 \cdot 10^{-3}$ |
| CYA | -1.2 | $7.26 \cdot 10^{-3}$ | $3.15 \cdot 10^{-2}$ | ZOR | -0.2 | $2.26 \cdot 10^{-4}$ | $2.89 \cdot 10^{-3}$ |
| ZOC | 0 | $5.25 \cdot 10^{-9}$ | $1.69 \cdot 10^{-7}$ | SMS | -0.6 | $6.65 \cdot 10^{-4}$ | $4.31 \cdot 10^{-3}$ |
| DOM ₁ | 0.1 | $6.54 \cdot 10^{-5}$ | $3.61 \cdot 10^{-4}$ | DOM ₂ | -0.1 | $3.94 \cdot 10^{-4}$ | $1.34 \cdot 10^{-3}$ |
| DOM ₃ | 0 | $4.06 \cdot 10^{-4}$ | $2.06 \cdot 10^{-3}$ | OXY | 0 | $6.78 \cdot 10^{-3}$ | $3.07 \cdot 10^{-2}$ |
| POM ₁ | -0.3 | $4.68 \cdot 10^{-4}$ | $2.27 \cdot 10^{-3}$ | POM ₂ | -0.3 | $7.80 \cdot 10^{-4}$ | $3.97 \cdot 10^{-3}$ |
| POM ₃ | -0.2 | $4.06 \cdot 10^{-4}$ | $2.06 \cdot 10^{-3}$ | NH ₄ | 0 | $4.66 \cdot 10^{-5}$ | $5.28 \cdot 10^{-4}$ |
| NO ₂ | 0 | $2.13 \cdot 10^{-5}$ | $3.42 \cdot 10^{-4}$ | NO ₃ | 0 | $4.04 \cdot 10^{-4}$ | $1.90 \cdot 10^{-3}$ |
| TIP | 0 | $1.45 \cdot 10^{-4}$ | $3.62 \cdot 10^{-4}$ | DSi | 0 | $1.81 \cdot 10^{-3}$ | $8.46 \cdot 10^{-3}$ |
| TA | 0 | $4.39 \cdot 10^{-2}$ | $2.65 \cdot 10^{-1}$ | pH | 0 | $1.14 \cdot 10^{-3}$ | $7.22 \cdot 10^{-3}$ |
| DIC | 0 | $8.49 \cdot 10^{-3}$ | $6.54 \cdot 10^{-2}$ | CO ₂ (aq) | 0 | $2.24 \cdot 10^{-3}$ | $1.65 \cdot 10^{-2}$ |

the following days, as the water temperature and active irradiance increase (Fig. 12), the net production shows an increase. However, it still remains negative. The net change of DIA shifts to a positive direction due to a combination of net input and net production, leading to a simulated increase in DIA biomass. This trend continues until day 130 when the maximum DIA biomass is reached (Fig. 10). The decline in DIA biomass simulated from day 130 onwards is due to a combination of factors.

605 Firstly, the input factor could be contributing to the decrease when the DIA biomass exceeds the concentration of DIA in input flow (0.447 mgC L^{-1} , Tab. 2, Fig. 10). Additionally, the net production rate is also playing a role (Fig. 11). Although photosynthesis rate is increasing with water temperature and active irradiance until day 179 (not shown here), it is not enough to compensate for the other processes occurring in the diatom population (days 150 - 170), resulting in an overall decrease in biomass. Despite the positive contributions of net input and net production on DIA biomass around day 175, a significant

610 decrease in biomass occurred due to zooplankton grazing (Fig. 11, red line). Two factors impact the zooplankton dynamics: water temperature and half-saturation constant of grazing (Eq. (27)). The optimal temperature for zooplankton is $25 \text{ }^\circ\text{C}$ and the half-saturation constant of grazing for zooplankton is set to 0.4 mgC L^{-1} . Then, an equilibrium of DIA biomass is simulated until day 260 (Fig. 10), which means that the net production and net input in DIA biomass are balanced by the grazing of zooplankton. The input in DIA biomass primarily contributes to the increase in DIA biomass from day 260 (Fig. 11). As the

615 water temperature and active irradiance decrease during this time, the net production of DIA decreases and changes to negative by day 292.

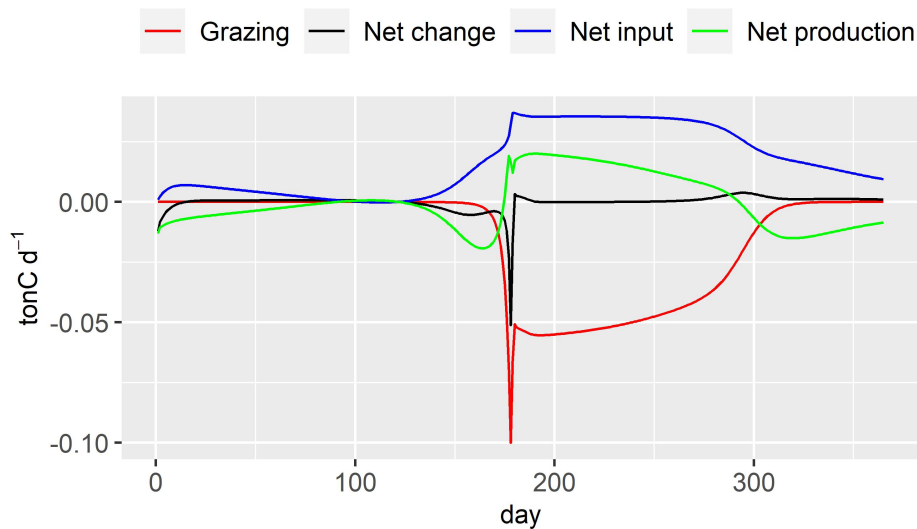


Figure 11. Budget fluxes of DIA (tonC d^{-1}). Grazing: Zooplankton grazing fluxes; Net production: Eq. (26); Net input: input flux - output flux; Net change: daily variation of DIA in the river stretch

The growth rate of large heterotrophic bacteria (LHB) increases (Fig. 13) with the increase of water temperature, causing a rise in LHB biomass until day 170 (Fig. 10). The fast decrease of small monomeric substrate (SMS) around day 175, synchronized with the grazing of zooplankton (Fig. 11), causes a decrease in growth rate of LHB. Its mortality rate is not impacted (not shown here). Consequently, this leads to a significant reduction in LHB biomass around day 175 (Fig. 10). The biomass of LHB remains stable until day 260. After that, it increases in conjunction with the rise in SMS concentration, which is synchronized with the increase in phytoplankton biomass.

4.2 Complexity and strengths of the RIVE model

Complexity can be understood in terms of the large number of variables represented and interacting with each other. The RIVE model is a multi-element, multi-form model and the kinetics it represents inevitably incorporate a large number of parameters. This is especially true as the RIVE model has opted for an explicit representation of the living communities (bacteria, phytoplankton, zooplankton, etc.) involved in the carbon and nutrient cycles. The model has thus become more complex over time and the addition of new processes (and therefore new parameters) has, as far as possible, been systematically based on experimental work in the laboratory or in the field to reduce the ranges of uncertainty around the kinetic parameters.

The RIVE model is designed as a tool for generating knowledge about the functioning of freshwater ecosystems and therefore it documents a large number of the biogeochemical processes, whether they are expressed weakly or strongly in a given freshwater ecosystem. The underlying hypothesis is that environmental factors control the intensity with which the various processes involved in the overall functioning of a hydrosystem are expressed.

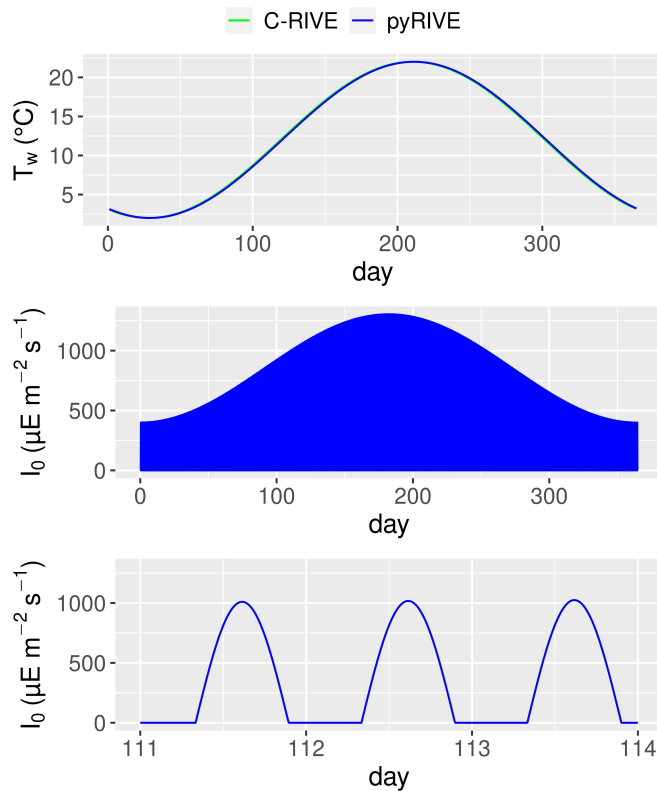


Figure 12. Simulated water temperature, active irradiance and zoom of active irradiance for days 111-114

Nevertheless, some work has specifically focused on analyzing the influence of RIVE parameters, particularly those controlling oxygen levels (Wang et al., 2018). This work identified key physical and physiological parameters. Based on the result of sensitivity analysis, a continuous oxygen data assimilation scheme has been developed (Prose-PA, (Wang et al., 2019, 2022)). The data assimilation allows to determine the physiological properties of microorganisms by integrating the associated uncertainties over time. The recent work of Hasanyar et al. (2023) has also helped to better quantify the sensitivity of oxygen to bacterial kinetics parameters as well as those relating to the composition of organic matter with the aims of parsimonious simplification of the number of parameters.

In these two examples, RIVE (C-RIVE) biogeochemical modelling is implemented in much more complex modelling platforms (particle filter, data assimilation, etc.) and the various analyses (sensitivity, uncertainties, etc.) are also supported by an overall assessment of the performance of the model applied to the Seine River.

4.3 Model limitations and future developments of unified RIVE

Currently, the unified RIVE v1.0 presented in this paper describes only the biogeochemical processes in water column. Comparison of benthic processes and simulations have not been investigated yet. Previous studies showed that sediment plays an



Figure 13. Large heterotrophic bacteria (LHB) dynamics and simulated concentrations of small monomeric substrate (SMS). Net change: daily variation of LHB in river stretch; Net input: input flux - output flux

important role on the metabolism of river (Vilmin et al., 2016) and lakes (Yan et al., 2022b). A unified sediment module should be further elaborated, based on existing modules (Even et al., 2004; Flipo et al., 2004; Thouvenot et al., 2007; Billen et al., 2015; Vilmin et al., 2015b) and implemented into unified RIVE. This sediment module will have to take into account not only the dissolved exchanges between the water column and the sediment but also the resuspension of particulates.

In addition, the unified RIVE v1.0 simulates phytoplankton dynamics, but periphyton or macrophyte development is not implemented in current versions. Flipo et al. (2004) showed that periphyton plays a major role in carbon cycling (primary productivity) in small rivers, not only in the carbon stock fixed at the bottom of the river but also in the carbon enrichment downstream of the river. These limitations should be considered in the future developments.

655 **4.4 Benefit of unified RIVE model**

The unified RIVE provides a set of governing equations of freshwater biogeochemical processes across different software platforms, such as pyNuts-Riverstrahler (Billen et al., 1994; Garnier et al., 1995; Thieu et al., 2017), PROSE-PA (Wang et al., 2019, 2023a), SWAT-RIVE (Manteaux et al., 2023, submitted), QUAL-NET (Minaudo et al., 2018), VEMALA V3 (Korppoo et al., 2017), Barman (Garnier et al., 2000; Thieu et al., 2006; Yan et al., 2022b), while incorporating the latest developments.

660 The unicity of the kinetics is important for facilitating and reinforcing the collaboration nationally or internationally within different research teams. Thanks to the unicity property formerly pointed out by the river continuum concept Vannote et al. (1980), the softwares based on unified RIVE can leverage on the already identified parameter values, regardless of the location in the network (Garnier et al., 2020). This feature is of great interest to the different research teams involved in freshwater quality research for instance river metabolism (Odum, 1956; Garnier and Billen, 2007; Escoffier et al., 2018; Gurung et al., 2019; Rodríguez-Castillo et al., 2019; Garnier et al., 2020; Segatto et al., 2020; Battin et al., 2023) or nutrient cycling (Garnier et al., 1999b; Alexander et al., 2002; Garnier et al., 2002; Billen et al., 2007; Lauerwald et al., 2013; Lindenschmidt et al., 2019; Maavara et al., 2020; Marescaux et al., 2020; Yan et al., 2022a).

Open science has become increasingly popular and even indispensable in scientific community as it allows for easier accessibility and the reproduction of the scientific results. The unified RIVE project, as an open-source project, allows for the dissemination and wider use of the RIVE biogeochemical model by creating a public repository with different programming languages.

670

5 Conclusions

This paper presents a conceptual freshwater biogeochemistry model: unified RIVE v1.0, programmed in Python 3 and ANSI C. The degradation of organic matter by heterotrophic bacteria, the dynamics of primary producer (phytoplankton) and zoo- plankton including carbon cycling and nutrient cycling are described exhaustively. In unified RIVE v1.0, the organic matter is degraded via bacteria activity, which is simulated by a HSB model. According to the results, the HSB model is able to model the organic matter degradation and bacterial dynamics in batch experiments. A case study is designed to compare the simulations of the two digital implementations (Python 3 for pyRIVE 1.0 and ANSI C for C-RIVE 0.32). These implementations simulate similar concentrations of all state variables including microorganisms, organic carbon, nutrients, and inorganic carbon.

675

680 The river stretch case study allows us to compare the two implementations of unified RIVE V1.0 under transient contrasting conditions involving complex biogeochemical cycles. The specific dynamics of each simulated species depend on different limiting factors. The calculation of photosynthesis of phytoplankton (diatoms, chlorophyceae, cyanobacteria) takes into account the light that naturally presents a day/night variation. The development of diatoms specifically takes into account the dissolved silica in the simulated environment. The growth of microorganisms depend on the quantity of nutrients (primary producer, nitrifying bacteria) and the small monomeric substrate (heterotrophic bacteria). In addition, the effect of water temperature is also taken into account for the physiology of the simulated microorganisms' communities (photosynthesis, growth, respiration, mortality).

Finally, unified RIVE being an open-source project, contributions from the freshwater biogeochemistry community are strongly encouraged to achieve a better understanding of freshwater ecosystem functioning and investigate further the future of river systems in a changing world.

Code availability. The C-RIVE 0.32 implements the unified RIVE v1.0 in ANSI C. It is available under Eclipse Public License 2.0 in the following Zenodo repository: <https://doi.org/10.5281/zenodo.7849609>; Wang et al. (2023b). pyRIVE 1.0 implements the unified RIVE v1.0 in Python 3 and is available under the Eclipse Public License 2.0 in InDoRES repository: <https://doi.org/10.48579/PRO/Z9ACPI>; Thieu et al. (2023).

Table A1. Various implementations of the RIVE model and its applications in different freshwater systems

| Freshwater systems | Climates | Software platforms | References |
|---|-------------|------------------------------|---|
| Danube River (Romania and Bulgaria) | Continental | Riverstrahler | Garnier et al. (2002) |
| Day-Nhue River (Vietnam) | Tropical | Seneque-Riverstrahler | Luu et al. (2021) |
| Grand Morin River (France) | Temperate | PROSE | Flipo et al. (2004, 2007) |
| Loire River (France) | Temperate | Grafts-Seneque/Riverstrahler | Garnier et al. (2018a) |
| Lot River (France) | Temperate | Grafts-Seneque/Riverstrahler | Garnier et al. (2018b) |
| Lule and Kalix rivers (Sweden) | Subarctic | Riverstrahler | Sferratore et al. (2008) |
| Mosel River (Germany) | Temperate | Riverstrahler | Garnier et al. (1999a) |
| Orgeval watershed (France) | Temperate | Seneque-Riverstrahler | Garnier et al. (2014) |
| Red River (China and Vietnam) | Tropical | Seneque-Riverstrahler | Le et al. (2010); Phuong Quynh et al. (2014); Le et al. (2015); Nguyen et al. (2016) |
| Scheldt River (Belgium and Netherlands) | Temperate | Seneque-Riverstrahler | Billen et al. (2005); Thieu et al. (2009) |
| Somme River (France) | Temperate | Seneque-Riverstrahler | Thieu et al. (2009, 2010) |
| Seine River (France) | Temperate | Seneque-Riverstrahler | Billen et al. (2007); Thieu et al. (2009, 2010); Romero et al. (2019) |
| Seine River (France) | Temperate | pyNuts-Riverstrahler | Thieu et al. (2017); Desmit et al. (2018); Raimonet et al. (2018); Marescaux et al. (2020) |
| Seine River (France) | Temperate | PROSE/PROSE-PA | Even et al. (1998, 2004, 2007); Raimonet et al. (2015); Vilmin et al. (2015b, a, 2016, 2018); Wang (2019); Wang et al. (2022) |
| Zenne River (Belgium) | Temperate | Seneque-Riverstrahler | Garnier et al. (2013) |
| Sand-pit lake, reservoirs (France) | Temperate | Barman | Garnier and Billen (1994); Garnier et al. (2000); Thieu et al. (2006); Yan et al. (2022a) |

Appendix B: Parameter values for unified RIVE v1.0

The 120 parameter values necessary for running unified RIVE v1.0 are provided hereafter.

Table B1. Heterotrophic bacteria related parameters

| Parameter | Description | Value | Unit |
|-------------------------|---|-------|------------------------|
| * $e_{max20,dom_1,lhb}$ | Maximal hydrolysis rate of DOM ₁ at 20 °C related to LHB | 0.75 | [h ⁻¹] |
| * $e_{max20,dom_1,shb}$ | Maximal hydrolysis rate of DOM ₁ at 20 °C related to SHB | 0.75 | [h ⁻¹] |
| * $e_{max20,dom_2,lhb}$ | Maximal hydrolysis rate of DOM ₂ at 20 °C related to LHB | 0.25 | [h ⁻¹] |
| * $e_{max20,dom_2,shb}$ | Maximal hydrolysis rate of DOM ₂ at 20 °C related to SHB | 0.25 | [h ⁻¹] |
| * $b_{max20,lhb}$ | Maximal substrate (SMS) uptake rate of LHB at 20 °C | 0.6 | [h ⁻¹] |
| * $b_{max20,shb}$ | Maximal substrate (SMS) uptake rate of SHB at 20 °C | 0.16 | [h ⁻¹] |
| Y_{lhb} | Growth yield of LHB | 0.25 | [-] |
| Y_{shb} | Growth yield of SHB | 0.25 | [-] |
| * $k_{d20,lhb}$ | Mortality rate of LHB at 20 °C | 0.05 | [h ⁻¹] |
| * $k_{d20,shb}$ | Mortality rate of SHB at 20 °C | 0.02 | [h ⁻¹] |
| vs_{shb} | Sinking velocity of LHB | 0.0 | [m h ⁻¹] |
| vs_{lhb} | Sinking velocity of LHB | 0.02 | [m h ⁻¹] |
| $T_{opt,shb}$ | Optimal temperature of SHB | 20 | °C |
| $T_{opt,lhb}$ | Optimal temperature of LHB | 22 | °C |
| σ_{shb} | Range of temperature for SHB | 17 | °C |
| σ_{lhb} | Range of temperature for LHB | 12 | °C |
| $K_{sms,lhb}$ | Half-saturation constant of LHB for small monomeric substrate | 0.1 | [mgC L ⁻¹] |
| $K_{sms,shb}$ | Half-saturation constant of SHB for small monomeric substrate | 0.1 | [mgC L ⁻¹] |
| $K_{dom_1,shb}$ | Half-saturation constant for DOM ₁ hydrolysis related to SHB | 0.25 | [mgC L ⁻¹] |
| $K_{dom_1,lhb}$ | Half-saturation constant for DOM ₁ hydrolysis related to LHB | 0.25 | [mgC L ⁻¹] |
| $K_{dom_2,shb}$ | Half-saturation constant for DOM ₂ hydrolysis related to SHB | 2.5 | [mgC L ⁻¹] |
| $K_{dom_2,lhb}$ | Half-saturation constant for DOM ₂ hydrolysis related to LHB | 2.5 | [mgC L ⁻¹] |

*: Parameters depend on water temperature and are multiplied by $f(T) = \frac{e^{-\frac{(T-T_{opt})^2}{\sigma^2}}}{e^{-\frac{(20-T_{opt})^2}{\sigma^2}}}$ where T is water temperature in °C.

Table B2. Nitrifying bacteria related parameters

| Parameter | Description | Value | Unit |
|---------------------|--|-------|-------------------------------------|
| * $\mu_{max20,aob}$ | Maximal growth rate of AOB at 20 °C | 0.07 | [h ⁻¹] |
| * $\mu_{max20,nob}$ | Maximal growth rate of NOB at 20 °C | 0.05 | [h ⁻¹] |
| $K_{o_2,aob}$ | Half-saturation constant of AOB for O ₂ | 0.64 | [mgO ₂ L ⁻¹] |
| $K_{o_2,nob}$ | Half-saturation constant of NOB for O ₂ | 1.088 | [mgO ₂ L ⁻¹] |
| $K_{nh_4,aob}$ | Half-saturation constant of AOB for NH ₄ ⁺ | 0.75 | [mgN L ⁻¹] |
| $K_{no_2,nob}$ | Half-saturation constant of NOB for NO ₂ ⁻ | 0.05 | [mgN L ⁻¹] |
| Y_{aob} | Growth yield of AOB | 0.07 | [mgC/mgN] |
| Y_{nob} | Growth yield of NOB | 0.02 | [mgC/mgN] |
| * $k_{d20,aob}$ | Mortality rate of AOB at 20 °C | 0.005 | [h ⁻¹] |
| * $k_{d20,nob}$ | Mortality rate of NOB at 20 °C | 0.005 | [h ⁻¹] |
| vs_{aob} | Sinking velocity of AOB | 0.005 | [m h ⁻¹] |
| vs_{nob} | Sinking velocity of NOB | 0.005 | [m h ⁻¹] |
| $T_{opt,aob}$ | Optimal temperature of AOB | 23 | [°C] |
| σ_{aob} | Range of temperature for NOB | 18 | [°C] |
| $T_{opt,nob}$ | Optimal temperature of NOB | 23 | [°C] |
| σ_{nob} | Range of temperature for NOB | 18 | [°C] |

*: Parameters depend on water temperature and are multiplied by $f(T) = \frac{e^{-\frac{(T-T_{opt})^2}{\sigma^2}}}{e^{-\frac{(20-T_{opt})^2}{\sigma^2}}}$ where T is water temperature in °C.

Table B3. Primary producer dynamics related parameters

| Parameter | Description | Value | Unit |
|---------------------|--|--------|---|
| * $P_{max20,dia}$ | Maximal photosynthesis rate of diatoms at 20 °C | 0.2 | [h ⁻¹] |
| * $P_{max20,gra}$ | Maximal photosynthesis rate of green algae at 20 °C | 0.25 | [h ⁻¹] |
| * $P_{max20,cya}$ | Maximal photosynthesis rate of cyanobacteria at 20 °C | 0.1 | [h ⁻¹] |
| α_{dia} | Photosynthetic efficiency of diatoms | 0.0012 | [h ⁻¹ ($\mu\text{E m}^{-2} \text{s}^{-1}$) ⁻¹] |
| α_{gra} | Photosynthetic efficiency of green algae | 0.0012 | [h ⁻¹ ($\mu\text{E m}^{-2} \text{s}^{-1}$) ⁻¹] |
| α_{cya} | Photosynthetic efficiency of cyanobacteria | 0.0012 | [h ⁻¹ ($\mu\text{E m}^{-2} \text{s}^{-1}$) ⁻¹] |
| β_{dia} | Photoinhibition capacity of diatoms | 0.0 | [h ⁻¹ ($\mu\text{E m}^{-2} \text{s}^{-1}$) ⁻¹] |
| β_{gra} | Photoinhibition capacity of green algae | 0.0 | [h ⁻¹ ($\mu\text{E m}^{-2} \text{s}^{-1}$) ⁻¹] |
| β_{cya} | Photoinhibition capacity of cyanobacteria | 0.0 | [h ⁻¹ ($\mu\text{E m}^{-2} \text{s}^{-1}$) ⁻¹] |
| η_{base} | Light extinction related coefficient for pure water | 0.2 | [m ⁻¹] |
| η_{chla} | Light algal self-shading light extinction coefficient | 0.02 | [m ⁻¹ ($\mu\text{gchla L}^{-1}$) ⁻¹] |
| η_{ss} | Light extinction coefficient related to suspended solid | 0.042 | [m ⁻¹ (mg L ⁻¹) ⁻¹] |
| * $\mu_{max20,dia}$ | Maximal growth rate of diatoms at 20 °C | 0.05 | [h ⁻¹] |
| * $\mu_{max20,gra}$ | Maximal growth rate of green algae at 20 °C | 0.05 | [h ⁻¹] |
| * $\mu_{max20,cya}$ | Maximal growth rate of cyanobacteria at 20 °C | 0.025 | [h ⁻¹] |
| $K_{S,dia}$ | Half-saturation constant for small precursors of diatoms | 0.06 | [-] |
| $K_{S,gra}$ | Half-saturation constant for small precursors of green algae | 0.06 | [-] |
| $K_{S,cya}$ | Half-saturation constant for small precursors of cyanobacteria | 0.06 | [-] |
| $K_{N,dia}$ | Half-saturation constant for nitrogen of diatoms | 0.014 | [mgN L ⁻¹] |
| $K_{N,gra}$ | Half-saturation constant for nitrogen of green algae | 0.014 | [mgN L ⁻¹] |
| $K_{N,cya}$ | Half-saturation constant for nitrogen of cyanobacteria | 0.014 | [mgN L ⁻¹] |
| $K_{P,dia}$ | Half-saturation constant for phosphorus of diatoms | 0.0155 | [mgP L ⁻¹] |
| $K_{P,gra}$ | Half-saturation constant for phosphorus of green algae | 0.062 | [mgP L ⁻¹] |
| $K_{P,cya}$ | Half-saturation constant for phosphorus of cyanobacteria | 0.062 | [mgP L ⁻¹] |
| $K_{Si,dia}$ | Half-saturation constant for silica of diatoms | 0.196 | [mgSi L ⁻¹] |
| * $R_{m20,dia}$ | Maintenance respiration coefficient of diatoms at 20 °C | 0.002 | [h ⁻¹] |
| * $R_{m20,gra}$ | Maintenance respiration coefficient of green algae at 20 °C | 0.002 | [h ⁻¹] |
| * $R_{m20,cya}$ | Maintenance respiration coefficient of cyanobacteria at 20 °C | 0.002 | [h ⁻¹] |
| $R_{\mu,dia}$ | Energetic cost of growth of diatoms | 0.5 | [-] |
| $R_{\mu,gra}$ | Energetic cost of growth of green algae | 0.5 | [-] |
| $R_{\mu,cya}$ | Energetic cost of growth of cyanobacteria | 0.5 | [-] |

*: Parameters depend on water temperature and are multiplied by $f(T) = \frac{e^{-\frac{(T-T_{opt})^2}{\sigma^2}}}{e^{-\frac{(20-T_{opt})^2}{\sigma^2}}}$ where T is water temperature in °C.

Table B3. Primary producer dynamics related parameters (continued)

| Parameter | Description | Value | Unit |
|-----------------------|--|-------|----------------------|
| $E_{cst, dia}$ | Basic excretion rate of diatoms | 0.006 | [h ⁻¹] |
| $E_{cst, gra}$ | Basic excretion rate of green algae | 0.006 | [h ⁻¹] |
| $E_{cst, cya}$ | Basic excretion rate of cyanobacteria | 0.006 | [h ⁻¹] |
| $E_{phot, dia}$ | Excretion constant of diatoms related to photosynthesis | 0.001 | [-] |
| $E_{phot, gra}$ | Excretion constant of green algae related to photosynthesis | 0.001 | [-] |
| $E_{phot, cya}$ | Excretion constant of cyanobacteria related to photosynthesis | 0.001 | [-] |
| * $S_{R, max20, dia}$ | Maximal rate of reserve products synthesis for diatoms at 20 °C | 0.15 | [h ⁻¹] |
| * $S_{R, max20, gra}$ | Maximal rate of reserve products synthesis for green algae at 20 °C | 0.2 | [h ⁻¹] |
| * $S_{R, max20, cya}$ | Maximal rate of reserve products synthesis for cyanobacteria at 20 °C | 0.075 | [h ⁻¹] |
| * $C_{R, max20, dia}$ | Maximal rate of reserve products catabolism for diatoms at 20 °C | 0.2 | [h ⁻¹] |
| * $C_{R, max20, gra}$ | Maximal rate of reserve products catabolism for green algae at 20 °C | 0.2 | [h ⁻¹] |
| * $C_{R, max20, cya}$ | Maximal rate of reserve products catabolism for cyanobacteria at 20 °C | 0.2 | [h ⁻¹] |
| * $k_{d20, dia}$ | Rate of diatoms mortality at 20 °C | 0.025 | [h ⁻¹] |
| * $k_{d20, gra}$ | Rate of green algae mortality at 20 °C | 0.025 | [h ⁻¹] |
| * $k_{d20, cya}$ | Rate of cyanobacteria mortality at 20 °C | 0.015 | [h ⁻¹] |
| vs_{dia} | Sinking velocity of diatoms | 0.006 | [m h ⁻¹] |
| vs_{gra} | Sinking velocity of green algae | 0.001 | [m h ⁻¹] |
| vs_{cya} | Sinking velocity of cyanobacteria | 0.006 | [m h ⁻¹] |
| $T_{opt, dia}$ | Optimal temperature of diatoms | 21 | [°C] |
| $T_{opt, gra}$ | Optimal temperature of green algae | 37 | [°C] |
| $T_{opt, cya}$ | Optimal temperature of cyanobacteria | 37 | [°C] |
| σ_{dia} | Range of temperature for diatoms | 13 | [°C] |
| σ_{gra} | Range of temperature for green algae | 15 | [°C] |
| σ_{cya} | Range of temperature for cyanobacteria | 12 | [°C] |

*: Parameters depend on water temperature and are multiplied by $f(T) = \frac{e^{-\frac{(T-T_{opt})^2}{\sigma^2}}}{e^{-\frac{(20-T_{opt})^2}{\sigma^2}}}$ where T is water temperature in °C.

Table B4. Organic matter dynamics parameters

| Parameter | Description | Value | Unit |
|--------------------|--|---------|--------------------|
| ϵ_{dom_1} | DOM ₁ fraction in lysis products | 0.2 | [-] |
| ϵ_{dom_2} | DOM ₂ fraction in lysis products | 0.2 | [-] |
| ϵ_{dom_3} | DOM ₃ fraction in lysis products | 0.1 | [-] |
| ϵ_{pom_1} | POM ₁ fraction in lysis products | 0.2 | [-] |
| ϵ_{pom_2} | POM ₂ fraction in lysis products | 0.2 | [-] |
| ϵ_{pom_3} | POM ₃ fraction in lysis products | 0.1 | [-] |
| * $k_{pom_1,20}$ | POM ₁ hydrolysis rate constant at 20 °C | 0.005 | [h ⁻¹] |
| k_{pom_2} | POM ₂ hydrolysis rate constant | 0.00025 | [h ⁻¹] |

*: Parameters depend on water temperature and are multiplied by $f(T) = \frac{e^{-\frac{(T-T_{opt})^2}{\sigma^2}}}{e^{-\frac{(20-T_{opt})^2}{\sigma^2}}}$

where T is water temperature in °C.

Table B5. Zooplankton parameters

| Parameter | Description | Value | Unit |
|---------------------|---|-------|------------------------|
| * $\mu_{max20,zor}$ | Maximal growth rate of ZOR at 20 °C | 0.025 | [h ⁻¹] |
| * $\mu_{max20,zoc}$ | Maximal growth rate of ZOC at 20 °C | 0.015 | [h ⁻¹] |
| * $b_{max20,zor}$ | Maximal grazing rate of ZOR at 20 °C | 0.1 | [h ⁻¹] |
| * $b_{max20,zoc}$ | Maximal grazing rate of ZOC at 20 °C | 0.05 | [h ⁻¹] |
| $K_{phy,zor}$ | Half-saturation constant for grazing phytoplankton of ZOR | 0.1 | [mgC L ⁻¹] |
| $K_{phy,zoc}$ | Half-saturation constant for grazing phytoplankton of ZOC | 0.1 | [mgC L ⁻¹] |
| $PHY_{0,zor}$ | Threshold phytoplankton concentration for grazing of ZOR | 0.1 | [mgC L ⁻¹] |
| $PHY_{0,zoc}$ | Threshold phytoplankton concentration for grazing of ZOC | 0.1 | [mgC L ⁻¹] |
| * $k_{d20,zor}$ | Mortality rate of ZOR at 20 °C | 0.007 | [h ⁻¹] |
| * $k_{d20,zoc}$ | Mortality rate of ZOC at 20 °C | 0.007 | [h ⁻¹] |
| $T_{opt,zor}$ | Optimal temperature of ZOR | 25 | [°C] |
| $T_{opt,zoc}$ | Optimal temperature of ZOC | 25 | [°C] |
| σ_{zor} | Range of temperature for ZOR | 10 | [°C] |
| σ_{zoc} | Range of temperature for ZOC | 10 | [°C] |
| vs_{zor} | Sinking velocity of ZOR | 0.02 | [m h ⁻¹] |
| vs_{zoc} | Sinking velocity of ZOC | 0.02 | [m h ⁻¹] |

*: Parameters depend on water temperature and are multiplied by $f(T) = \frac{e^{-\frac{(T-T_{opt})^2}{\sigma^2}}}{e^{-\frac{(20-T_{opt})^2}{\sigma^2}}}$ where T is water temperature in °C.

Table B6. Phosphate and Silica related parameters

| Parameter | Description | Value | Unit |
|--|---|---------|------------------------|
| <i>Phosphate adsorption desorption</i> | | | |
| P_{ac} | Maximal adsorption capacity of mineral suspended solids (MSS) | 0.00558 | [mgP/mgMSS] |
| K_{ps} | Half saturation adsorption constant | 0.682 | [mgP L ⁻¹] |
| <i>Silica dynamiques</i> | | | |
| Kb_{Si20} | Biogenic silica dissolution rate at 20 °C | 0.0001 | [h ⁻¹] |

Author contributions. **Shuaitao Wang:** Conceptualization, Methodology, Software, Validation, Formal analysis, Investigation, Visualization, Writing – original draft. **Vincent Thieu:** Conceptualization, Methodology, Software, Formal analysis, Writing - Review & Editing, Supervision. **Gilles Billen:** Conceptualization, Methodology, Data curation, Formal analysis, Writing - Review & Editing. **Josette Garnier:** Conceptualization, Data curation, Formal analysis, Writing - Review & Editing. **Marie Silvestre:** Software, Writing - Review & Editing.

Audrey Marescaux: Conceptualization, Software. **Xingcheng Yan:** Software. **Nicolas Flipo:** Conceptualization, Methodology, Formal analysis, Software, Writing - Review & Editing, Supervision, Funding acquisition.

705 *Competing interests.* The authors declare that they have no known competing financial interests or personal relationships that could have appeared to influence the work reported in this paper.

Acknowledgements. This work was carried out under the PIREN-Seine program (<https://www.piren-seine.fr/>), part of the french Long Term Socio-Ecological Research (LTSER) (named in France "Zone Atelier Seine" (INEE, CNRS). We thank Lou Weidenfeld, Benjamin Mercier and Anun Marninez for carrying organic matter batch experiments.

710 Particularly, we would like to dedicate this paper to the memory of Pr. Pierre Servais: his knowledge, expertise, and passion for this field of study will continue to guide us in the pursuit of our scientific work.

References

- Aissa-Grouz, N., Garnier, J., and Billen, G.: Long trend reduction of phosphorus wastewater loading in the Seine: determination of phosphorus speciation and sorption for modeling algal growth, *Environmental Science and Pollution Research*, <https://doi.org/10.1007/s11356-016-7555-7>, 2016.
- 715 Alexander, R. B., Elliott, A. H., Shankar, U., and McBride, G. B.: Estimating the sources and transport of nutrients in the Waikato River Basin, New Zealand, *Water Resources Research*, 38, 4–1–4–23, <https://doi.org/10.1029/2001WR000878>, 2002.
- Azam, F., Fenchel, T., Gray, J., Meyer, L., and Thingstad, F.: The Ecological Role of Water-Column Microbes in the Sea, *Marine Ecology Progress Series*, 10, 257–263, 1983.
- Battin, T. J., Lauerwald, R., Bernhardt, E. S., Bertuzzo, E., Gener, L. G., Hall, R. O., Hotchkiss, E. R., Maavara, T., Pavelsky, T. M., Ran, L.,
720 Raymond, P., Rosentreter, J. A., and Regnier, P.: River Ecosystem Metabolism and Carbon Biogeochemistry in a Changing World, *Nature*, 613, 449–459, <https://doi.org/10.1038/s41586-022-05500-8>, 2023.
- Billen, G.: Protein degradation in Aquatic Environments, in: *Microbial Enzyme in Aquatic Environments*, edited by Chrost, R., Springer Verlag, Berlin, 1991.
- Billen, G. and Servais, P.: Modélisation des processus de dégradation bactérienne de la matière organique en milieu aquatique, in: *Micro-organismes dans les écosystèmes océaniques*, edited by et al., B., pp. 219–245, Masson Paris, 1989.
- 725 Billen, G., Servais, P., and Fontigny, A.: Growth and mortality in bacterial populations dynamics of aquatic environments, *Arch. Hydrobiol. Beih. Ergebn. Limnol*, 31, 173–183, 1988.
- Billen, G., Servais, P., and Becquevort, S.: Dynamics of bacterioplankton in oligotrophic and eutrophic aquatic environments: bottom-up or top-down control?, in: *Fluxes Between Trophic Levels and Through the Water-Sediments Interface*, edited by Bonin, D. and Golterman, H., pp. 37–42, Kluwer Academic Publishers, 1990.
- 730 Billen, G., Garnier, J., and Hanset, P.: Modelling phytoplankton development in whole drainage networks: the RIVERSTRAHLER Model applied to the Seine river system, *Hydrobiologia*, 289, 119–137, 1994.
- Billen, G., Garnier, J., and Rousseau, V.: Nutrient fluxes and water quality in the drainage network of the Scheldt basin over the last 50 year, *Hydrobiologia*, 540, 47–67, 2005.
- 735 Billen, G., Garnier, J., Mouchel, J.-M., and Silvestre, M.: The Seine system: Introduction to a multidisciplinary approach of the functioning of a regional river system, *Sciences of Total Environment*, 375, 1–12, 2007.
- Billen, G., Garnier, J., and Silvestre, M.: A simplified algorithm for calculating benthic nutrient fluxes in river systems, *Ann. Limnol. - Int. J. Lim.*, 51, 37–47, <https://doi.org/10.1051/limn/2014030>, 2015.
- Brion, N. and Billen, G.: Une réévaluation de la méthode de mesure de l'activité nitrifiante autotrophe par la méthode d'incorporation de bicarbonate marqué $\text{H}^{14}\text{CO}_3^-$ et son application pour estimer des biomasses de bactéries nitrifiantes, *Revue des Sciences de l'Eau*, 11, 283–302, 1998.
- 740 Conley, D. J., Kilham, S. S., and Theriot, E.: Differences in silica content between marine and freshwater diatoms, *Limnology and Oceanography*, 34, 205–212, <https://doi.org/10.4319/lo.1989.34.1.0205>, 1989.
- Culbertson, C. H.: Calculation of the in situ pH of seawater¹, *Limnology and Oceanography*, 25, 150–152, <https://doi.org/10.4319/lo.1980.25.1.0150>, 1980.
- 745

- Desmit, X., Thieu, V., Billen, G., Campuzano, F., Dulière, V., Garnier, J., Lassaletta, L., Ménesguen, A., Neves, R., Pinto, L., Silvestre, M., Sobrinho, J., and Lacroix, G.: Reducing marine eutrophication may require a paradigmatic change, *Science of the Total Environment*, 635, 1444–1466, <https://doi.org/10.1016/j.scitotenv.2018.04.181>, 2018.
- 750 Escoffier, N., Bensoussan, N., Vilmin, L., Flipo, N., Rocher, V., David, A., Métivier, F., and Groleau, A.: Estimating ecosystem metabolism from continuous multi-sensor measurements in the Seine River, *Environmental Science and Pollution Research*, 25, 23 451–23 467, <https://doi.org/10.1007/s11356-016-7096-0>, 2018.
- Even, S., Poulin, M., Garnier, J., Billen, G., Servais, P., Chesterikoff, A., and Coste, M.: River ecosystem modelling: Application of the PROSE model to the Seine river (France), *Hydrobiologia*, 373, 27–45, <https://doi.org/10.1023/A:1017045522336>, 1998.
- 755 Even, S., Poulin, M., Mouchel, J. M., Seidl, M., and Servais, P.: Modelling oxygen deficits in the Seine river downstream of combined sewer overflows, *Ecol. Model.*, 173, 177–196, 2004.
- Even, S., Mouchel, J. M., Servais, P., Flipo, N., Poulin, M., Blanc, S., Chabanel, M., and Paffoni, C.: Modeling the impacts of Combined Sewer Overflows on the river Seine water quality, *Sciences of Total Environment*, 375, 140–151, <https://doi.org/10.1016/j.scitotenv.2006.12.007>, 2007.
- Fick, A.: Ueber diffusion, *Annalen der Physik und Chemie*, J.A. Barth, 1855.
- 760 Flipo, N., Even, S., Poulin, M., Tusseau-Vuillemin, M. H., Améziane, T., and Dauta, A.: Biogeochemical Modelling at the River Scale: Plankton and Periphyton Dynamics - Grand Morin case study, France, *Ecol. Model.*, 176, 333–347, 2004.
- Flipo, N., Rabouille, C., Poulin, M., Even, S., Tusseau-Vuillemin, M. H., and Lalande, M.: Primary production in headwater streams of the Seine basin: the Grand Morin case study, *Sciences of Total Environment*, 375, 98–109, <https://doi.org/10.1016/j.scitotenv.2006.12.015>, 2007.
- 765 Fontigny, A., Billen, G., and Vives-Rego, J.: Some kinetic characteristics of exoproteolytic activity in coastal seawater, *Estuarine Coastal and Shelf Science*, 25, 127–133, [https://doi.org/10.1016/0272-7714\(87\)90030-8](https://doi.org/10.1016/0272-7714(87)90030-8), 1987.
- Fuhrman, J. and Azam, F.: Thymidine Incorporation as a Measure of Heterotrophic Bacterioplankton Production in Marine Surface Waters: Evaluation and Field Results, *Marine Biology*, 66, 109–120, 1982.
- 770 Garnier, J. and Billen, G.: Ecological interactions in a shallow sand-pit lake (Lake Créteil, Parisian Basin, France): a modelling approach, *Hydrobiologia*, 275/276, 97–114, 1994.
- Garnier, J. and Billen, G.: Production vs. Respiration in river systems: An indicator of an "ecological status", *Science of the Total Environment*, 375, 110–124, <https://doi.org/10.1016/j.scitotenv.2006.12.006>, 2007.
- Garnier, J., Billen, G., and Servais, P.: Physiological characteristics and ecological role of small- and large-sized bacteria in a polluted river (Seine River, France), *Arch. Hydrobiol. Beih.*, 37, 83–94, 1992a.
- 775 Garnier, J., Servais, P., and Billen, G.: Bacterioplankton in the Seine river (France): impact of the Parisian urban effluent, *Can. J. Microbiol.*, 38, 56–64, 1992b.
- Garnier, J., Billen, G., and Coste, M.: Seasonal succession of diatoms and chlorophyceae in the drainage network of the river Seine: Observations and modelling, *Limnol. Oceanogr.*, 40, 750–765, 1995.
- 780 Garnier, J., Billen, G., Hanset, P., Testard, P., and Coste, M.: Développement algal et eutrophisation dans le réseau hydrographique de la Seine, in: *La Seine en son bassin-Fonctionnement écologique d'un système fluvial anthropisé*, edited by Meybeck, M., de Marsily, G., and Fustec, E., pp. 593–626, Elsevier, 1998.

- Garnier, J., Billen, G., and Palfner, L.: Understanding the Oxygen Budget and Related Ecological Processes in the River Mosel: The RIVER-STRAHLER Approach, in: *Man and River Systems*, edited by Garnier, J. and Mouchel, J.-M., pp. 151–166, Springer Netherlands, Dordrecht, https://doi.org/10.1007/978-94-017-2163-9_17, 1999a.
- 785 Garnier, J., Leporcq, B., Sanchez, N., and Philippon, X.: Biogeochemical mass-balances (C, N, P, Si) in three large reservoirs of the Seine Basin (France), *Biogeochemistry*, 47, 119–146, <https://doi.org/10.1023/A:1006101318417>, 1999b.
- Garnier, J., Billen, G., Sanchez, N., and Leporcq, B.: Ecological functioning of the Marne Reservoir (upper Seine basin, France), *Regul. Rivers: Res. Mgmt.*, 16, 51–71, 2000.
- Garnier, J., Billen, G., Hannon, E., Fonbonne, S., Videnina, Y., and Soulie, M.: Modeling transfer and retention of nutrients in the drainage
790 network of the Danube River, *Estuar. Coast. Shelf*, 54, 285–308, 2002.
- Garnier, J., Brion, N., Callens, J., Passy, P., Deligne, C., Billen, G., Servais, P., and Billen, C.: Modeling historical changes in nutrient delivery and water quality of the Zenne River (1790s–2010): The role of land use, waterscape and urban wastewater management, *Journal of Marine Systems*, 128, 62–76, <https://doi.org/10.1016/j.jmarsys.2012.04.001>, 2013.
- Garnier, J., Billen, G., Vilain, G., Benoit, M., Passy, P., Tallec, G., Tournebize, J., Anglade, J., Billy, C., Mercier, B., Ansart,
795 P., Azougui, A., Sebilo, M., and Kao, C.: Curative vs. preventive management of nitrogen transfers in rural areas: Lessons from the case of the Orgeval watershed (Seine River basin, France), *Journal of Environmental Management*, 144, 125–134, <https://doi.org/10.1016/j.jenvman.2014.04.030>, 2014.
- Garnier, J., Ramarson, A., Billen, G., Théry, S., Thiéry, D., Thieu, V., Minaudo, C., and Moatar, F.: Nutrient inputs and hydrology together determine biogeochemical status of the Loire River (France): Current situation and possible future scenarios, *Science of The Total Environment*, 637–638, 609–624, <https://doi.org/10.1016/j.scitotenv.2018.05.045>, 2018a.
- 800 Garnier, J., Ramarson, A., Thieu, V., Némery, J., Théry, S., Billen, G., and Coynel, A.: How can water quality be improved when the urban waste water directive has been fulfilled? A case study of the Lot river (France), *Environmental Science and Pollution Research*, 25, 11 924–11 939, <https://doi.org/10.1007/s11356-018-1428-1>, 2018b.
- Garnier, J., Marescaux, A., Guillon, S., Vilmin, L., Rocher, V., Billen, G., Thieu, V., Silvestre, M., Passy, P., Raimonet, M., Groleau, A.,
805 Théry, S., Tallec, G., and Flipo, N.: The Handbook of Environmental Chemistry, chap. Ecological Functioning of the Seine River: From Long-Term Modelling Approaches to High-Frequency Data Analysis, pp. 1–28, *Handbook of Environmental Chemistry*, Springer, Berlin, Heidelberg, <https://doi.org/10.1007/978-2019-379>, 2020.
- Garnier, J., Weidenfeld, L., Billen, G., Martinez, A., Mercier, B., Rocher, V., Tabuchi, J.-P., and Azimi, S.: La matière organique dans le continuum terrestre-aquatique du bassin de la Seine, *Rapport annuel PIREN-Seine*, PIREN-Seine,
810 <https://doi.org/10.26047/PIREN.rapp.ann.2021.vol21>, 2021.
- Gurung, A., Iwata, T., Nakano, D., and Urabe, J.: River Metabolism along a Latitudinal Gradient across Japan and in a global scale, *Scientific Reports*, 9, <https://doi.org/10.1038/s41598-019-41427-3>, 2019.
- Gypens, N., Lancelot, C., and Borges, A. V.: Carbon dynamics and CO₂ air-sea exchanges in the eutrophied coastal waters of the Southern Bight of the North Sea: a modelling study, *Biogeosciences*, 1, 147–157, <https://doi.org/10.5194/bg-1-147-2004>, 2004.
- 815 Hasanyar, M., Romary, T., Wang, S., and Flipo, N.: How much do bacterial growth properties and biodegradable dissolved organic matter control water quality at low flow?, *Biogeosciences*, 20, 1621–1633, <https://doi.org/10.5194/bg-20-1621-2023>, 2023.
- Hellweger, F. L.: 100 Years since Streeter and Phelps: It Is Time To Update the Biology in Our Water Quality Models, *Environmental Science & Technology*, 49, 6372–6373, <https://doi.org/10.1021/acs.est.5b02130>, 2015.

- Jähne, B., Heinz, G., and Dietrich, W.: Measurement of the diffusion coefficients of sparingly soluble gases in water, *Journal of Geophysical Research: Oceans*, 92, 10 767–10 776, <https://doi.org/10.1029/JC092iC10p10767>, 1987.
- 820 Korpoo, M., Huttunen, M., Huttunen, I., Piirainen, V., and Vehviläinen, B.: Simulation of bioavailable phosphorus and nitrogen loading in an agricultural river basin in Finland using VEMALA v.3, *Journal of Hydrology*, 549, 363–373, <https://doi.org/10.1016/j.jhydrol.2017.03.050>, 2017.
- Lancelot, C., Veth, C., and Mathot, S.: Modelling ice-edge phytoplankton bloom in the Scotia-Weddell sea sector of the southern ocean during spring 1998, *J. Mar. System*, 2, 333–346, 1991.
- 825 Lauerwald, R., Hartmann, J., Moosdorf, N., Dürr, H. H., and Kempe, S.: Retention of dissolved silica within the fluvial system of the conterminous USA, *Biogeochemistry*, 112, 637–659, 2013.
- Le, T. P. Q., Billen, G., Garnier, J., Théry, S., Ruelland, D., Anh, N. X., and Van, M. C.: Nutrient (N, P, Si) transfers in the subtropical Red River system (China and Vietnam): Modelling and budget of nutrient sources and sinks, *Journal of Asian Earth Sciences*, 37, 259 – 274, <https://doi.org/10.1016/j.jseaes.2009.08.010>, 2010.
- 830 Le, T. P. Q., Billen, G., Garnier, J., and Chau, V.: Long-term biogeochemical functioning of the Red River (Vietnam): past and present situations, *Reg. Environ. Change*, 15, 329–339, <https://doi.org/10.1007/s10113-014-0646-4>, 2015.
- Lindenschmidt, K.-E., Carr, M. K., Sadeghian, A., and Morales-Marin, L.: CE-QUAL-W2 model of dam outflow elevation impact on temperature, dissolved oxygen and nutrients in a reservoir, *Scientific Data*, 6, 312, <https://doi.org/10.1038/s41597-019-0316-y>, 2019.
- 835 Luu, M. T., Dinh, T. D., Trinh, D. A., and Doc, N. T.: Water Quality in an Urbanized River Basin Impacted by Multi-Pollution Sources: From Comprehensive Surveys to Modelling, *ScienceAsia*, 47, 86, <https://doi.org/10.2306/scienceasia1513-1874.2021.014>, 2021.
- Maavara, T., Chen, Q., Van Meter, K., Brown, L. E., Zhang, J., Ni, J., and Zarfl, C.: River dam impacts on biogeochemical cycling, *Nature Reviews Earth & Environment*, 1, 103–116, <https://doi.org/10.1038/s43017-019-0019-0>, 2020.
- Manteaux, S., Sauvage, S., Samie, R., Monteil, C., Garnier, J., Thieu, V., Cakir, R., and Sánchez-Pérez, J.-M.: Modeling in-stream biogeochemical processes at catchment scale: Coupling SWAT and RIVE models, *Environmental Modelling & Software*, p. 105856, <https://doi.org/10.1016/j.envsoft.2023.105856>, 2023.
- 840 Marescaux, A., Thieu, V., Gypens, N., Silvestre, M., and Garnier, J.: Modeling inorganic carbon dynamics in the Seine River continuum in France, *Hydrology and Earth System Sciences*, 24, 2379–2398, <https://doi.org/10.5194/hess-24-2379-2020>, 2020.
- Michaelis, L. and Menten, M. L.: Die kinetik der invertinwirkung - The kinetics of invertin action, *Biochemische Zeitschrift*, 49, 333–369, 1913.
- 845 Minaudo, C., Curie, F., Jullian, Y., Gassama, N., and Moatar, F.: QUAL-NET, a high temporal-resolution eutrophication model for large hydrographic networks, *Biogeosciences*, 15, 2251–2269, <https://doi.org/10.5194/bg-15-2251-2018>, 2018.
- Monod, J.: The growth of bacterial cultures, *Annual Review of Microbiology*, 3, 371–394, <https://doi.org/10.1146/annurev.mi.03.100149.002103>, 1949.
- 850 Nguyen, H. T. M., Billen, G., Garnier, J., Rochelle-Newall, E., Ribolzi, O., Servais, P., and Le, T. P. Q.: Modelling of faecal indicator bacteria (FIB) in the Red River basin (Vietnam), *Environmental Monitoring and Assessment*, <https://doi.org/10.1007/s10661-016-5528-4>, 2016.
- Odum, H. T.: Primary production in Flowing waters, *Limnol. Oceanogr.*, 1, 795–801, 1956.
- Phuong Quynh, T. L., Garnier, J., Billen, G., Lam Ngoc, T., and Chau Van, M.: Preliminary results of riverstrahler model application to the red river system (Vietnam), *Vietnam Journal of Chemistry*, 47, 110, <https://doi.org/10.15625/4550>, 2014.
- 855 Platt, T., Gallegos, C., and Harrison, W.: Photoinhibition of photosynthesis in natural assemblages of marine phytoplankton, *J. Mar. Res.*, 38, 687–701, 1980.

- Raimonet, M., Vilmin, L., Flipo, N., Rocher, V., and Laverman, A.: Modelling the fate of nitrite in an urbanized river using experimentally obtained nitrifier growth parameters, *Water Research*, 73, 373–387, <https://doi.org/10.1016/j.watres.2015.01.026>, 2015.
- 860 Raimonet, M., Thieu, V., Silvestre, M., Oudin, L., Rabouille, C., Vautard, R., and Garnier, J.: Landward perspective of coastal eutrophication potential under future climate change: The Seine River case (France), *Frontiers in Marine Science*, 5, 136, <https://doi.org/10.3389/fmars.2018.00136>, 2018.
- Redfield, A., Ketchum, B., and Richards, F.: *The Sea. Ideas and Observations on Progress in the Study of the Seas. The Composition of the Sea-Water Comparative and Descriptive Oceanography*, vol. 2, chap. The influence of organisms on the composition of sea-water, pp. 26–77, Interscience Publishers, 1963.
- 865 Rego, J. V., Billen, G., Fontigny, A., and Somville, M.: Free and Attached proteolytic activity in water environments, *Marine Ecology Progress Series*, 21, 245–249, 1985.
- Rickert, D., Schlüter, M., and Wallmann, K.: Dissolution kinetics of biogenic silica from the water column to the sediments, *Geochimica et Cosmochimica Acta*, 66, 439–455, [https://doi.org/10.1016/S0016-7037\(01\)00757-8](https://doi.org/10.1016/S0016-7037(01)00757-8), 2002.
- Rodríguez-Castillo, T., Estévez, E., González-Ferreras, A., and Barquín, J.: Estimating Ecosystem Metabolism to Entire River Networks, *Ecosystems*, 22, 892–911, <https://doi.org/10.1007/s10021-018-0311-8>, 2019.
- 870 Romero, E., Garnier, J., Billen, G., Ramarson, A., Riou, P., and Le Gendre, R.: Modeling the biogeochemical functioning of the Seine estuary and its coastal zone: Export, retention, and transformations, *Limnology and Oceanography*, 64, 895–912, <https://doi.org/10.1002/lno.11082>, 2019.
- Ruelland, D., Billen, G., Brunstein, D., and Garnier, J.: SENEQUE: a multi-scaling GIS interface to the Riverstrahler model of the biogeochemical functioning of river systems., *The Science of the total environment*, 375, 257–73, <https://doi.org/10.1016/j.scitotenv.2006.12.014>, 2007.
- 875 Segatto, P., Battin, T., and Bertuzzo, E.: Modeling the coupled dynamics of stream metabolism and microbial biomass, *Limnology and Oceanography*, 65, 1573–1593, <https://doi.org/10.1002/lno.11407>, 2020.
- Servais, P. and Garnier, J.: Contribution of Heterotrophic Bacterial Production to the Carbon Budget of the River Seine (France), *Microb. Ecol.*, 25, 19–33, 1993.
- 880 Servais, P., Billen, G., and Vives-Rego, J.: Rate of Bacterial Mortality in Aquatic Environments, *Appl. envir. Microbiol.*, 49, 1448–1454, 1985.
- Servais, P., Billen, G., and Hascoët, M.-C.: Determination of the biodegradable fraction of dissolved organic matter in waters, *Water Research*, 21, 445–450, 1987.
- 885 Servais, P., Billen, G., Martinez, J., and Vives-Rego, J.: Estimating bacterial mortality by the disappearance of ³H-labeled intracellular DNA, *FEMS Microbiology Letters*, 62, 119–125, [https://doi.org/10.1016/0378-1097\(89\)90021-9](https://doi.org/10.1016/0378-1097(89)90021-9), 1989.
- Servais, P., Barillier, A., and Garnier, J.: Determination of the biodegradable fraction of dissolved and particulate organic carbon in waters, *Ann. Limnol. - Int. J. Limn.*, 31, 75–80, <https://doi.org/10.1051/limn/1995005>, 1995.
- Servais, P., Billen, G., Goncalves, A., and Garcia-Armisen, T.: Modelling microbiological water quality in the Seine river drainage network: 890 past, present and future situations, *Hydrology and Earth System Sciences*, 11, 1581–1592, <https://doi.org/10.5194/hess-11-1581-2007>, 2007.
- Sferratore, A., Billen, G., Garnier, J., Smedberg, E., Humborg, C., and Rahm, L.: Modelling nutrient fluxes from sub-arctic basins: Comparison of pristine vs. dammed rivers, *Journal of Marine Systems*, 73, 236–249, <https://doi.org/10.1016/j.jmarsys.2007.10.012>, 2008.
- Somville, M. and Billen, G.: A method for determining exoproteolytic activity in natural water, *Limnol. Oceanogr.*, 28, 190–193, 1983.

- 895 Streeter, H. and Phelps, E. B.: A study of the pollution and natural purification of the Ohio River, Tech. Rep. 146, U.S. Public Health Service, Treasury Department, Washington DC, 1925.
- Stumm, W. and Morgan, J.: Aquatic Chemistry: Chemical Equilibria and Rates in Natural Waters, A Wiley-interscience publication, Wiley, 1996.
- Thieu, V., Guillon, T., Billen, G., Garnier, J., and Thouvenot, M.: Applicatif BARMAN - Notice d'utilisation., Rapport annuel PIREN-Seine, 900 PIREN-Seine, <https://doi.org/10.26047/PIREN.rapp.ann.2006.vol07>, 2006.
- Thieu, V., Billen, G., and Garnier, J.: Nutrient transfer in three contrasting NW European watersheds: The Seine, Somme, and Scheldt Rivers. A comparative application of the Seneque/Riverstrahler model, *Water Research*, 43, 1740–1754, <https://doi.org/10.1016/j.watres.2009.01.014>, 2009.
- Thieu, V., Mayorga, E., Billen, G., and Garnier, J.: Subregional and downscaled global scenarios of nutrient transfer in river basins: Seine- 905 Somme-Scheldt case study, *Global Biogeochemical Cycles*, 24, <https://doi.org/10.1029/2009GB003561>, 2010.
- Thieu, V., Silvestre, M., Garnier, J., and Billen, G.: Introducing the biogeochemical pynuts-riverstrahler model to assess prospective scenario impact along the aquatic continuum in western eu-rivers, in: Proceedings of ASLO Aquatic Sciences Meeting: "Moutains to the Sea", Honolulu, USA, 2017.
- Thieu, V., Silvestre, M., Wang, S., Marescaux, A., Yan, X., Garnier, J., and Billen, G.: pyRIVE, <https://doi.org/10.48579/PRO/Z9ACP1>, 910 2023.
- Thouvenot, M., Billen, G., and Garnier, J.: Modelling nutrient exchange at the sediment-water interface of river systems, *Journal of Hydrology*, 341, 55–78, 2007.
- Vannote, R., Minshall, G. W., Cummins, K., Sedell, J., and Cushing, C.: The River Continuum Concept, *Can. J. Fish. Aquat. Sci.*, 37, 130–137, <https://doi.org/10.1139/f80-017>, 1980.
- 915 Vilmin, L., Aissa-Grouz, N., Garnier, J., Billen, G., Mouchel, J. M., Poulin, M., and Flipo, N.: Impact of hydro-sedimentary processes on the dynamics of soluble reactive phosphorus in the Seine River, *Biogeochemistry*, 122, 229–251, <https://doi.org/10.1007/s10533-014-0038-3>, 2015a.
- Vilmin, L., Flipo, N., de Fouquet, C., and Poulin, M.: Pluri-annual sediment budget in a navigated river system: The Seine River (France), *Sciences of Total Environment*, 502, 48–59, <https://doi.org/10.1016/j.scitotenv.2014.08.110>, 2015b.
- 920 Vilmin, L., Flipo, N., Escoffier, N., Rocher, V., and Groleau, A.: Carbon fate in a large temperate human-impacted river system: Focus on benthic dynamics, *Global Biogeochem. Cycles*, 30, 1086–1104, <https://doi.org/10.1002/2015GB005271>, 2016.
- Vilmin, L., Flipo, N., Escoffier, N., and Groleau, A.: Estimation of the water quality of a large urbanized river as defined by the European WFD: what is the optimal sampling frequency?, *Environmental Science and Pollution Research*, 25, 23 485–23 501, <https://doi.org/10.1007/s11356-016-7109-z>, 2018.
- 925 Wang, S.: Simulation du métabolisme de la Seine par assimilation de données en continu, Theses, Mines Paris – PSL, <https://pastel.archives-ouvertes.fr/tel-02388690>, 2019.
- Wang, S., Flipo, N., and Romary, T.: Time-dependent global sensitivity analysis of the C-RIVE biogeochemical model in contrasted hydro-logical and trophic contexts, *Water Research*, 144, 341–355, <https://doi.org/10.1016/j.watres.2018.07.033>, 2018.
- Wang, S., Flipo, N., and Romary, T.: Oxygen data assimilation for estimating micro-organism communities' parameters in river systems, 930 *Water Research*, 165, 115 021, <https://doi.org/10.1016/j.watres.2019.115021>, 2019.
- Wang, S., Flipo, N., Romary, T., and Hasanyar, M.: Particle filter for high frequency oxygen data assimilation in river systems, *Environmental Modelling & Software*, p. 105382, <https://doi.org/10.1016/j.envsoft.2022.105382>, 2022.

- Wang, S., Flipo, N., and Romary, T.: Which filter for data assimilation in water quality models? Focus on oxygen reaeration and heterotrophic bacteria activity, *Journal of Hydrology*, 620, 129–143, <https://doi.org/10.1016/j.jhydrol.2023.129423>, 2023a.
- 935 Wang, S., Vilmin, L., Hasanyar, M., and Flipo, N.: C-RIVE, <https://doi.org/10.5281/zenodo.7849609>, 2023b.
- Wanninkhof, R.: Relationship between wind speed and gas exchange over the ocean, *Journal of Geophysical Research: Oceans*, 97, 7373–7382, <https://doi.org/10.1029/92JC00188>, 1992.
- Weiss, R.: Carbon dioxide in water and seawater: the solubility of a non-ideal gas, *Marine Chemistry*, 2, 203–215, [https://doi.org/10.1016/0304-4203\(74\)90015-2](https://doi.org/10.1016/0304-4203(74)90015-2), 1974.
- 940 Wilke, C. R. and Chang, P.: Correlation of diffusion coefficients in dilute solutions, *AIChE Journal*, 1, 264–270, <https://doi.org/10.1002/aic.690010222>, 1955.
- Yan, X., Garnier, J., Billen, G., Wang, S., and Thieu, V.: Unravelling nutrient fate and CO₂ concentrations in the reservoirs of the Seine Basin using a modelling approach, *Water Research*, 225, 119–135, <https://doi.org/10.1016/j.watres.2022.119135>, 2022a.
- Yan, X., Thieu, V., Wu, S., and Garnier, J.: Reservoirs change pCO₂ and water quality of downstream rivers: Evidence from three reservoirs
945 in the Seine Basin, *Water Research*, 213, 118–158, <https://doi.org/10.1016/j.watres.2022.118158>, 2022b.